Integrated design of a lower limb rehabilitation mechanism using differential evolution

José Saúl Muñoz-Reina[a], Miguel Gabriel Villarreal-Cervantes[a,*], Leonel Germán Corona-Ramírez[b]

[a] *Optimal Mechatronic Design Laboratory, Postgraduate department, Mechatronic Section, Centro de Innovación y Desarrollo Tecnológico en Cómputo, Instituto Politécnico Nacional, CDMX, Mexico.*
[b] *Unidad Profesional Interdisciplinaria en Ingeniería y Tecnologías Avanzadas, Instituto Politécnico Nacional, CDMX, Mexico*

Abstract

In the last years, one degree of freedom mechanisms has been incorporated into rehabilitation machines. Their designs usually involve kinematic synthesis leaving aside their complex dynamic nature. An integrated methodology to design a one degree of freedom eight-bar mechanism for lower limb rehabilitation is presented in this paper. The methodology simultaneously considers kinematic synthesis, structure shape design, and dynamic performance. A non-linear constrained dynamic optimization problem is proposed where the design objective relates the accuracy in the prescribed movement and the energy consumption reduction. This problem is solved by using different differential evolution variants for finding the most suitable synergistic solution. The results show that the obtained design can follow the path with 52.13% less energy consumption compared to a design that does not consider such integration. This also results in less control effort, and hence the velocity regulation accuracy is improved. The three-dimensional printed prototype illustrates the obtained solution.

Keywords: Concurrent design, integrated design, rehabilitation mechanism, kinematic synthesis, structure shape design, dynamic performance.

1. Introduction

Lower limb injuries are the most frequent disabilities for different factors such as traffic accidents, sports injuries, aging, degenerative diseases, and unhealthy lifestyle. Therefore, rehabilitation therapy is a crucial factor to maintain, recover and develop the movement of the affected limbs through exercise routines with a minimum interaction of the physiotherapist.

In the last years, specialized robotic systems positively improve rehabilitation process and reduce the recovery time, maximizing the performance of the affected corporal area. Those systems can be divided according to the applied motion to the patient's body, the exoskeleton and the end-effector systems [1]. The exoskeleton systems move limb joints through a mechanical structure that is fixed on the patient limb and, therefore, the structure can move each part of the limb e.g., the Lokomat robot. Those systems are the high-cost alternatives to reduce the patient

*Corresponding author
Email address: mvillarrealc@ipn.mx (Miguel Gabriel Villarreal-Cervantes)

recovery time and enhance the skeletal muscle regeneration of the affected limb. On the other hand, in the end-effector systems, the movement is only carried out in the injured area, with the help of support providing specific trajectories similar to the natural movement. As the end-effector systems provide particular movements, the use of mechanisms is increasing because they can perform the particular motion and build them with low-cost and easy-operation features. For instance, four-bar mechanisms, six and ten-bar mechanisms, and cam-linkage seven-bar crank-slider mechanism have been synthesized to follow several precision points described by the gait's ankle trajectory. The kinematic synthesis in those works is generally stated as an optimization problem. The performance function is related to the kinematic performance based on the tracking error between a point into the mechanism and a prescribed trajectory. The solution to the problem has been firstly addressed with gradient-based techniques and in recent years with Evolutionary Algorithms (EAs). The latter is less likely to get stuck at local minima, and they are not sensitive to initial conditions. They are also free derivative, and they can endow easily, outstanding features of other algorithms. That features make a better exploration and exploitation in the solution search such that a better synergy in the design solution can be achieved [2].

The main feature in the lower limb rehabilitation mechanism design as end-effector systems is in the synthesis process. Usually, the kinematic synthesis based on optimization does not consider the dynamic response. This results in designs that require more energy consumption, implying a significant control effort to perform the task. Consequently, the advanced control design should be used to compensate for the highly nonlinear dynamic behavior [3]. In this direction, the mechatronic design approach, also called Concurrent Design, has motivated the combination of mechanical and electrical engineering with software engineering into a single design step to improve the obtained design solution synergically [4]. The optimal balance in the design specifications of different domains results in mechatronic systems with an enhanced synergy [5, 6, 2, 7]. This synergy has shown advantages in the mechatronic system performance over a traditional design, where the latter fulfills each design requirement in a separate design step [8, 9, 10]. One of the mechatronic design frameworks is to design the mechanical structure such that the control system is benefited. In [5], the Design For Control (DFC) approach is developed where the reduction of the shaking force/moment of the system facilitates the control design. In [11], the bond graphs and the genetic programming are combined to improve the complex multi-domain system features related to the mechanical part. Hence, according to [5] and [11], the mechanical structure positively influences the control design whether suitable performance indexes are considered.

Most of the work related to the lower limb rehabilitation mechanism is traditionally designed based on the kinematic synthesis, ignoring the dynamic characteristics that can influence the control performance. Even the patient's lower limb weight can largely influence the mechanism dynamic behavior and may produce a mechanical failure in joints. Also, the existing synthesis techniques in the lower limb rehabilitation mechanism do not take into account the simultaneous integration of the link shape, which should provide efficient inertial properties of links to minimize the control effort and, thus, the energy consumption. The structural shape requires other processes to obtain from the inertial properties the corresponding link shape. Some examples of such processes are the discretization into small mass elements of a predefined shape and the systematic placement of them along the link length [12], the maximization of the external

work constrained by the volume of all links [13], the use of topology optimization [14], among others.

Hence, this paper proposes integrating the kinematic synthesis, the structure shape design, and the dynamics into the design of one degree of freedom ($d.o.f$) eight-bar mechanism for the lower limb rehabilitation to reduce the energy consumption simultaneously. Thus, a simple controller can suitably regulate the system with less control effort in the next design stage. The design approach is based on the average anthropometry for the Mexican population. It is formulated as a mono-objective optimization problem where the combination of design objectives is through the weighted sum approach employing eight Differential Evolution variants for finding the most suitable synergistic design. Inverse dynamic analysis of the lower limb rehabilitation mechanism with a stress analysis verifies the obtained design. A comparative study with a traditional design, where only the kinematic synthesis is considered, shows outstanding results of the proposed integrated design methodology. The experimental result in a scaled prototype visualizes the obtained solution.

The paper is structured as follows: In Section 2 the kinematics and dynamics analysis for the lower limb rehabilitation mechanism are detailed. The optimization problem statement for the integrated design methodology called concurrent design is given in Section 3 and the solvers (Differential Evolution variants) are described in Section 4. The results and discussion are provided in Section 5. Finally, in Section 6 the conclusions are drawn.

2. Kinematics and dynamics analysis

The sketch of the one degree of freedom eight-bar rehabilitation mechanism is shown in Fig. 1(a), where $\vec{l_s}\ \forall\ s = \{1, 2, \ldots, 9\}$ and $\vec{l'_s}\ \forall\ s = \{6, 8\}$ represent link position vectors with magnitudes of l_s, l'_s and orientations of θ_s, θ'_s. The $(\bar{x}_E, \bar{y}_E)$ is the desired path to be followed by the point (x_E, y_E) in the mechanism by completing a revolution of the crank link 2. The foot of the patient is placed on the point (x_E, y_E); hence the corresponding exerted force is given by $\vec{F}_{K8}$. In the next sub-sections, the rehabilitation mechanism is splitted into two four-bar mechanisms ($M_1 = \{\vec{l_2}, \vec{l_5}, \vec{l'_6}, \vec{l_9}\}$ and $M_2 = \{\vec{l_1}, \vec{l_2}, \vec{l_3}, \vec{l_4}\}$) and one five-bar mechanism ($M_3 = \{\vec{l_4}, \vec{l_6}, \vec{l_7}, \vec{l_8}, \vec{l_{12}}\}$) to obtain the overall kinematics and dynamics.

2.1. Position analysis

From position vector loop equations (1)-(3) of sub-mechanisms M_1, M_2 and M_3, the angular positions θ_i and $\theta'_6\ \forall\ i = \{3, 4, 5, 7, 8\}$ of links are obtained, and they are presented in (S1)-(S6) of the Supplementary Material.

$$l_2 e^{j\theta_2} + l_5 e^{j\theta_5} - l'_6 e^{j\theta'_6} - l_9 e^{j\theta_9} = 0 \quad (1)$$

$$l_2 e^{j\theta_2} + l_3 e^{j\theta_3} - l_4 e^{j\theta_4} - l_1 e^{j\theta_1} = 0 \quad (2)$$

$$l_6 e^{j\theta_6} + l_7 e^{j\theta_7} - l_8 e^{j\theta_8} - l_4 e^{j\theta_4} - l_{12} e^{j\theta_{12}} = 0 \quad (3)$$

2.2. Velocity analysis

The angular velocities $\omega_s\ \forall\ s = \{3, ..., 8\}$ of links, given by (S29)-(S34) in the Supplementary Material, are obtained as follows: From the time derivatives of position vector loop equations (1)-(3), the velocity vector loop equations (4)-(6)

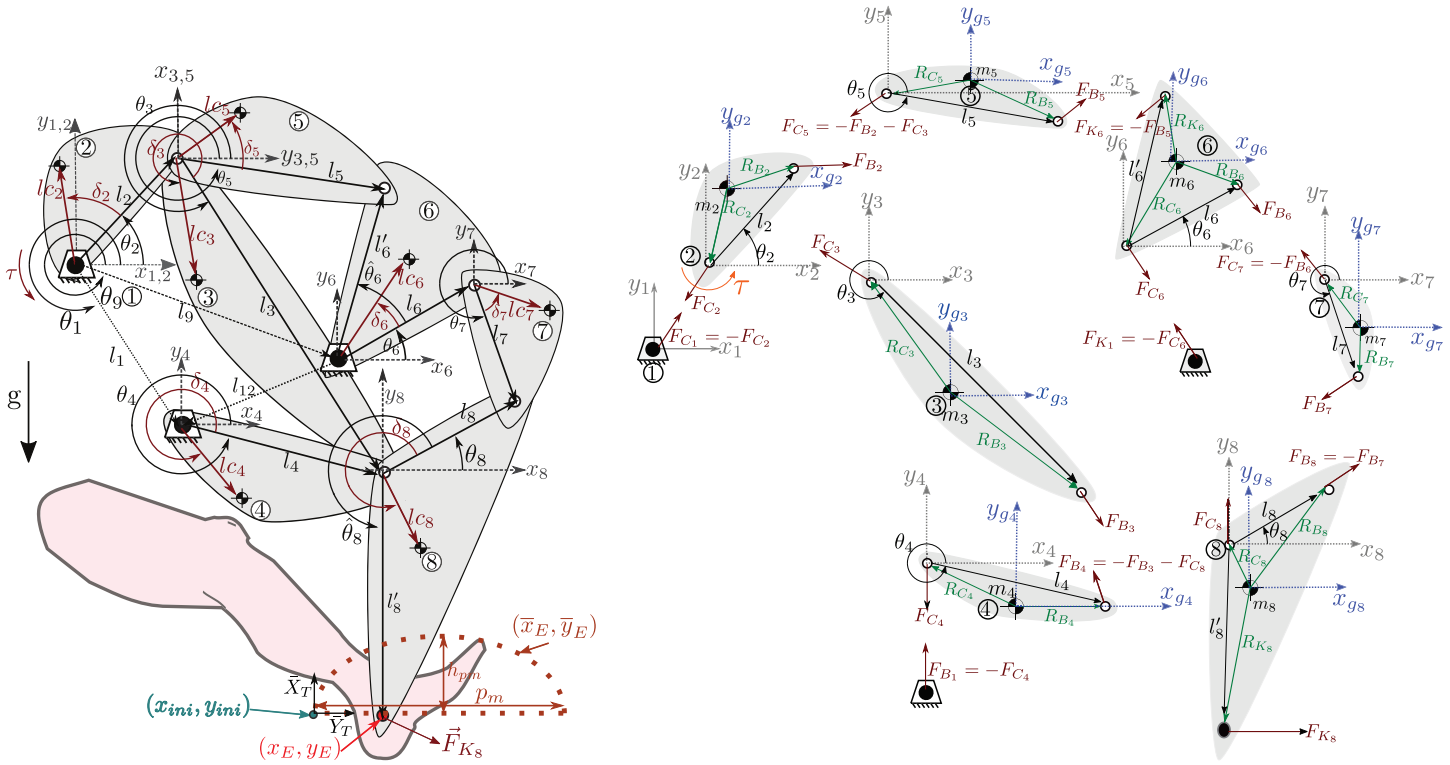

(a) Sketch (b) Free-body diagram

Figure 1: Sketch of the eight-bar rehabilitation mechanism with its free-body diagram representation for each link.

are set for each sub-mechanism M_1, M_2 and M_3. Then, using the Euler's formula and separating in equations the real and imaginary part, the angular velocities ω_s can be obtained by solving such equation system.

$$jl_2e^{j\theta_2}\omega_2 + jl_5e^{j\theta_5}\omega_5 - jl'_6e^{j\theta'_6}\omega_6 = 0 \quad (4)$$

$$jl_2e^{j\theta_2}\omega_2 + jl_3e^{j\theta_3}\omega_3 - jl_4e^{j\theta_4}\omega_4 = 0 \quad (5)$$

$$j\omega_6l_6e^{j\theta_6} + j\omega_7l_7e^{j\theta_7} - j\omega_8l_8e^{j\theta_8} - j\omega_4l_4e^{j\theta_4} = 0 \quad (6)$$

2.3. Acceleration analysis

This analysis involves the angular acceleration of links and the mass center's linear ones because these are required for the dynamic analysis presented in Section 2.4.

2.3.1. Angular acceleration

The angular accelerations α_s $\forall s = \{3, ..., 8\}$ of links, given by (S35)-(S40) in the Supplementary Material, are obtained through a similar procedure given above, but now, the system of equations is provided by the acceleration

vector loop equations (7)-(9) for each sub-mechanism (M_1, M_2 and M_3).

$$-l_2e^{j\theta_2}\omega_2^2 + l_2je^{j\theta_2}\alpha_2 - l_5e^{j\theta_5}\omega_5^2 + l_5je^{j\theta_5}\alpha_5 + l'_6e^{j\theta'_6}\omega_6^2 - l'_6je^{j\theta'_6}\alpha_6 = \quad 0 \tag{7}$$

$$-l_2e^{j\theta_2}\omega_2^2 + l_2je^{j\theta_2}\alpha_2 - l_3e^{j\theta_3}\omega_3^2 + l_3je^{j\theta_3}\alpha_3 + l_4e^{j\theta_4}\omega_4^2 - l_4je^{j\theta_4}\alpha_4 = \quad 0 \tag{8}$$

$$-l_6e^{j\theta_6}\omega_6^2 + l_6je^{j\theta_6}\alpha_6 - l_7e^{j\theta_7}\omega_7^2 + l_7je^{j\theta_7}\alpha_7 + l_8e^{j\theta_8}\omega_8^2 - l_8je^{j\theta_8}\alpha_8 + l_4e^{j\theta_4}\omega_4^2 - l_4je^{j\theta_4}\alpha_4 = \quad 0 \tag{9}$$

2.3.2. Linear acceleration

The linear acceleration $\vec{a}_{G_s} = [a_{G_{s_x}}, a_{G_{s_y}}]^T$ of the $s-th$ link mass center $\forall\ s = \{2, 3, ..., 8\}$ is obtained through the second derivative of the mass center position vector with respect to the inertial coordinate $x_1 - y_1$. Then, the linear accelerations in polar coordinates are shown in (10)-(16), where lc_s and δ_s are the position and orientation of the mass center related to the $s-th$ coordinate frame.

$$\vec{a}_{G_2} = lc_2e^{j(\theta_2+\delta_2)}(j\alpha_2 - \omega_2^2) \tag{10}$$

$$\vec{a}_{G_3} = l_2e^{j\theta_2}(j\alpha_2 - \omega_2^2) + lc_3e^{j(\theta_3+\delta_3)}(j\alpha_3 - \omega_3^2) \tag{11}$$

$$\vec{a}_{G_4} = lc_4e^{j(\theta_4+\delta_4)}(j\alpha_4 - \omega_4^2) \tag{12}$$

$$\vec{a}_{G_5} = l_2e^{j\theta_2}(j\alpha_2 - \omega_2^2) + lc_5e^{j(\theta_5+\delta_5)}(j\alpha_5 - \omega_5^2) \tag{13}$$

$$\vec{a}_{G_6} = lc_6e^{j(\theta_6+\delta_6)}(j\alpha_6 - \omega_6^2) \tag{14}$$

$$\vec{a}_{G_7} = l_6e^{j\theta_6}(j\alpha_6 - \omega_2^6) + lc_7e^{j(\theta_7+\delta_7)}(j\alpha_7 - \omega_7^2) \tag{15}$$

$$\vec{a}_{G_8} = l_4e^{j\theta_4}(j\alpha_4 - \omega_4^2) + lc_8e^{j(\theta_8+\delta_8)}(j\alpha_8 - \omega_8^2) \tag{16}$$

2.4. Dynamics analysis

In order to obtain the dynamics of the eight-bar rehabilitation mechanism, the applied forces $\vec{F}_{\hat{k}_s} = [F_{\hat{k}_{s_x}}, F_{\hat{k}_{s_y}}]^T$ and torque τ; and the corresponding position vectors $\vec{R}_{\hat{k}_s} = [R_{\hat{k}_{s_x}}, R_{\hat{k}_{s_y}}]^T\ \forall\ s = \{2, ..., 8\} \wedge \hat{k} = \{B, C, K\}$ with respect to the $s-th$ link mass center, are visualized on each link in a Free-Body Diagram (FBD) in Fig. 1(b). The elements of the $s-th$ vector $\vec{R}_{\hat{k}_s}$ are given in (S41)-(S56) of the Supplementary Material.

By using the Newton's second law in each link's Free-body diagram and considering the coordinate system $x_{g_s} - y_{g_s}$ and also the rotation axis in z_{g_s}, the dynamics equations are obtained. Those dynamics are represented in (17)-(37), where m_s is the $s-th$ link mass, I_{sG} is the $s-th$ link inertia moment and g is the gravity acceleration.

The force and torque analysis in the FBD of link two is represented by:

$$F_{C_{2_x}} + F_{B_{2_x}} = m_2a_{G_{2x}} \tag{17}$$

$$F_{C_{2_y}} + F_{B_{2_y}} = m_2a_{G_{2y}} + m_2g \tag{18}$$

$$\tau + R_{C_{2_x}}F_{C_{2_y}} - R_{C_{2_y}}F_{C_{2_x}} + R_{B_{2_x}}F_{B_{2_y}} - R_{B_{2_y}}F_{B_{2_x}} = I_{2_G}\alpha_2 \tag{19}$$

The force and torque analysis in the FBD of link three is represented by:

$$F_{C_{3_x}} + F_{B_{3_x}} = m_3 a_{G_{3x}} \tag{20}$$

$$F_{C_{3_y}} + F_{B_{3_y}} = m_3 a_{G_{3y}} + m_3 g \tag{21}$$

$$R_{C_{3_x}} F_{C_{3_y}} - R_{C_{3_y}} F_{C_{3_x}} + R_{B_{3_x}} F_{B_{3_y}} - R_{B_{3_y}} F_{B_{3_x}} = I_{3_G} \alpha_3 \tag{22}$$

The force and torque analysis in the FBD of link four is represented by:

$$F_{C_{4_x}} - F_{B_{3_x}} - F_{C_{8_x}} = m_4 a_{G_{4x}} \tag{23}$$

$$F_{C_{4_y}} - F_{B_{3_y}} - F_{C_{8_y}} = m_4 a_{G_{4y}} + m_4 g \tag{24}$$

$$R_{C_{4_x}} F_{C_{4_y}} - R_{C_{4_y}} F_{C_{4_x}} - R_{B_{4_x}} F_{B_{3_y}} + R_{B_{4_y}} F_{B_{3_x}} - R_{B_{4_x}} F_{C_{8_y}} + R_{B_{4_y}} F_{C_{8_x}} = I_{4_G} \alpha_4 \tag{25}$$

The force and torque analysis in the FBD of link five is represented by:

$$F_{B_{5_x}} - F_{B_{2_x}} - F_{C_{3_x}} = m_5 a_{G_{5x}} \tag{26}$$

$$F_{B_{5_y}} - F_{B_{2_y}} - F_{C_{3_y}} = m_5 a_{G_{5y}} + m_5 g \tag{27}$$

$$R_{B_{5_x}} F_{B_{5_y}} - R_{B_{5_y}} F_{B_{5_x}} - R_{C_{5_x}} F_{B_{2_y}} + R_{C_{5_y}} F_{B_{2_x}} - R_{C_{5_x}} F_{C_{3_y}} + R_{C_{5_y}} F_{C_{3_x}} = I_{5_G} \alpha_5 \tag{28}$$

The force and torque analysis in the FBD of link six is represented by:

$$F_{C_{6_x}} + F_{B_{6_x}} - F_{B_{5_x}} = m_6 a_{G_{6x}} \tag{29}$$

$$F_{C_{6_y}} + F_{B_{6_y}} - F_{B_{5_y}} = m_6 a_{G_{6y}} + m_6 g \tag{30}$$

$$R_{C_{6_x}} F_{C_{6_y}} - R_{C_{6_y}} F_{C_{6_x}} + R_{B_{6_x}} F_{B_{6_y}} - R_{B_{6_y}} F_{B_{6_x}} - R_{K_{6_x}} F_{B_{5_y}} + R_{K_{6_y}} F_{B_{5_x}} = I_{6_G} \alpha_6 \tag{31}$$

The force and torque analysis in the FBD of link seven is represented by:

$$F_{B_{7_x}} - F_{B_{6_x}} = m_7 a_{G_{7x}} \tag{32}$$

$$F_{B_{7_y}} - F_{B_{6_y}} = m_7 a_{G_{7y}} + m_7 g \tag{33}$$

$$R_{B_{7_x}} F_{B_{7_y}} - R_{B_{7_y}} F_{B_{7_x}} - R_{C_{7_x}} F_{B_{6_y}} + R_{C_{7_y}} F_{B_{6_x}} = I_{7_G} \alpha_7 \tag{34}$$

The force and torque analysis in the FBD of link eight is represented by:

$$F_{K_{8_x}} + F_{C_{8_x}} - F_{B_{7_x}} = m_8 a_{G_{8x}} \tag{35}$$

$$F_{K_{8_y}} + F_{C_{8_y}} - F_{B_{7_y}} = m_8 a_{G_{8y}} + m_8 g \tag{36}$$

$$R_{K_{8_x}} F_{K_{8_y}} - R_{K_{8_y}} F_{K_{8_x}} + R_{C_{8_x}} F_{C_{8_y}} - R_{C_{8_y}} F_{C_{8_x}} - R_{B_{8_x}} F_{B_{7_y}} + R_{B_{8_y}} F_{B_{7_x}} = I_{8_G} \alpha_8 \tag{37}$$

The inverse dynamic model of the rehabilitation mechanism can be reduced as $\check{X} = \check{A}^{-1}\check{B}$ by grouping (17)-(37). The matrix $\check{A} \in R^{21\times 21}$ and the vector $\check{B} \in R^{21}$ are described in (S57)-(S58) of the Supplementary Material and $\check{X} \in R^{21}$ is described in (38).

$$\begin{aligned}\check{X} = [&F_{C_{2_x}} \quad F_{C_{2_y}} \quad F_{B_{2_x}} \quad F_{B_{2_y}} \quad F_{C_{3_x}} \quad F_{C_{3_y}} \quad F_{B_{3_x}} \quad F_{B_{3_y}} \quad F_{C_{4_x}} F_{C_{4_y}} \quad F_{B_{5_x}} \quad F_{B_{5_y}} \quad F_{C_{6_x}} \quad F_{C_{6_y}} \\ &F_{B_{6_x}} \quad F_{B_{6_y}} \quad F_{B_{7_x}} F_{B_{7_y}} \quad F_{C_{8_x}} \quad F_{C_{8_y}} \quad \tau]^T\end{aligned} \tag{38}$$

It is important to remark that the force applied in the (x_E, y_E) coordinate of the mechanism (see Fig. 1(a)) and the

crank angular velocity ω_2, are chosen as $\vec{F}_{K_8} = [0, -133.41]^T N$ and $\omega_2 = 2\pi\ rad/s$ (with acceleration of $\alpha_2 = 0\ rad/s^2$), respectively. Those values are considered in Section 5 for the design analysis of a complete rehabilitation mechanism cycle. The force $\vec{F}_{K_8}$ is set by considering the maximum mass of the Mexican population's lower limb [15], which results from 16% of the maximum corporal mass (85 kg). Besides, the angular velocity ω_2 represents the maximum speed for the rehabilitation trajectory cycle.

3. Concurrent design of the rehabilitation mechanism

The rehabilitation mechanism design simultaneously considers the dimensional synthesis, the structure shape design, and the dynamic performance in a single design step. This design is stated as an optimization problem where the spatial and temporal requirements are taken into account to improve the movement quality and energy consumption. In the next subsections, the details of the optimization problem are given.

3.1. Objective functions

The main dimensional synthesis goal is to follow twenty desired precision points of a semi-ellipse trajectory [16]. The continuous closed-trajectory can track a similar semi-ellipse trajectory fulfilling such points. Then, the precision point tracking error shown in (39) is one of the design objectives to be optimized, where $\bar{e} = [[\bar{x}_E, \bar{y}_E] - [x_E, y_E]]^T$ and t_f is the final time.

$$\bar{J}_1 = \frac{1}{t_f} \int_0^{t_f} \bar{e}^T \cdot \bar{e} \cdot dt \tag{39}$$

On the other hand, the mechanism's dynamic performance is influenced by the link mass redistribution, which directly affects energy consumption, the driving torque variation, and peak-to-peak magnitude. Assuming that the crank link has constant velocity, the energy consumption is related to the input torque. Hence, the average of the applied torque in the crank of the rehabilitation mechanism (the load presented in the mechanism dynamics) is the second design objective to be included as is displayed in (40).

$$\bar{J}_2 = \frac{1}{t_f} \int_0^{t_f} \tau^2 \cdot dt \tag{40}$$

3.2. Design variables

The design variables include the kinematic vector $\tilde{p}_{ki} = [l_1, l_2, ..., l_9, l'_6, l'_8, \theta_1, \theta_9, \hat{\theta}_6,\ \hat{\theta}_8, x_{ini}, y_{ini}, \theta_2(t_0), \theta_2(t_1), ..., \theta_2(t_f)]^T \in R^{17+\tilde{N}}$ and the shape vector $\tilde{p}_{sh} = [b_2, ..., b_8, c_2, ..., c_8, d_2, ..., d_8, e_2, ..., e_8, f_2, ..., f_8, g_2, ..., g_8, h_2, ..., h_8, i_2, ..., i_8, j_2, ..., j_8, k_2, ..., k_8]^T \in R^{70}$. The kinematic parameters are represented by the link lengths $\vec{l}_s\ \forall\ s = \{1, 2, ..., 9\}$ and $\vec{l}'_s\ \forall\ s = \{6, 8\}$; the link angles θ_1, θ_9, $\hat{\theta}_6$ and $\hat{\theta}_8$; the origin (x_{ini}, y_{ini}) of the coordinate system $\bar{X}_T - \bar{Y}_T$ where the desired trajectory is performed (see Fig. 1(a)); and the angular displacement of the crank $\theta_2(t)$ where the time is $t = 0, t_f/(\tilde{N}-1), ..., it_f/(\tilde{N}-1) \in [0, t_f]$, $\forall i = 0, 1, ..., \tilde{N}-1$ with $t_f = 1\ s$ as the average time to complete the gait cycle [17] and $\tilde{N}$ as the number of precision points. In this paper, octagonal prisms are considered as link shapes. So,

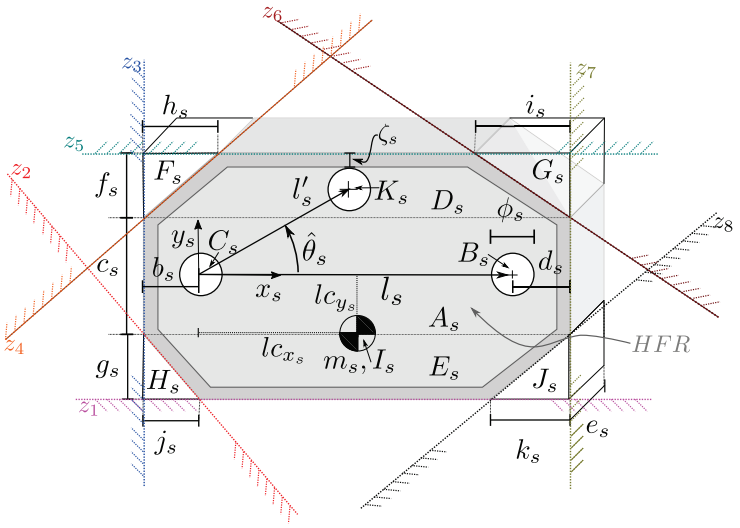

Figure 2: Octagonal link shape.

the shape parameters are the edges of the octagonal prism as is shown in Fig. 2. Two different links are considered: binary links (sixth and eighth links) and ternary links (second to fifth links and seventh link). The binary links have twelve parameters $(l_s, b_s, c_s, d_s, e_s, f_s, g_s, h_s, i_s, j_s, k_s, \phi_s)$ whereas the ternary links additionally include the length l'_s and the angle $\hat{\theta}_s$.

Therefore, the design variable vector $p \in R^{87+\tilde{N}}$ is given in (41). It is important to mention that this vector changes the link mass distribution (the dynamic parameters of the $s-th$ link i.e., mass m_s, mass center vector $\vec{lc}_s = [lc_{x_s}, lc_{y_s}]$ and inertia I_s) and as a consequence, the dynamic behavior of the mechanism can be modified.

$$p = [p_{ki}, p_{sh}]^T \tag{41}$$

Simple geometries are considered to simplify the dynamic parameter computation in terms of shape parameters. In the dynamic parameters, the aluminum density $\rho_s = 2710Kg/m^3$ is selected, and the diameter $\phi_s = 0.01905m$ is set for all link holes.

3.2.1. Mass

The mass m_s of the $s-th$ link is presented in (42), where $m_{k_s}\ \forall\ k = \{A, B, ..., H, J, K\}$ is the mass of the $k-th$ simple geometry.

$$m_s = m_{A_s} - m_{B_s} - m_{C_s} + m_{D_s} + m_{E_s} - m_{F_s} - m_{G_s} - m_{H_s} - m_{J_s} - m_{K_s} \tag{42}$$

where:

$$\begin{aligned}
&m_{A_s} = \rho_s \cdot (l_s + b_s + d_s) \cdot c_s \cdot e_s \quad && m_{C_s} = m_{B_s} = \tfrac{\rho_s \cdot \pi \cdot \phi_s^2 \cdot e_s}{4} && m_{D_s} = \rho_s \cdot (l_s + b_s + d_s) \cdot f_s \cdot e_s \\
&m_{E_s} = \rho_s \cdot (l_s + b_s + d_s) \cdot g_s \cdot e_s && m_{F_s} = \tfrac{\rho_s \cdot h_s \cdot f_s \cdot e_s}{2} && m_{G_s} = \tfrac{\rho_s \cdot i_s \cdot f_s \cdot e_s}{2} \\
&m_{H_s} = \tfrac{\rho_s \cdot j_s \cdot g_s \cdot e_s}{2} && m_{J_s} = \tfrac{\rho_s \cdot k_s \cdot g_s \cdot e_s}{2} && m_{K_s} = \begin{cases} \tfrac{\rho_s \cdot \pi \cdot \phi_s^2 \cdot e_s}{4} & \text{if } s = 6, 8 \\ 0 & \text{Otherwise} \end{cases}
\end{aligned} \tag{43}$$

3.2.2. Mass center

The mass center coordinates (lc_{x_s}, lc_{y_s}) are presented in (44).

$$\begin{aligned} lc_{x_s} =& \frac{1}{m_s}(x_{A_s} \cdot m_{A_s} - x_{B_s} \cdot m_{B_s} - x_{C_s} \cdot m_{C_s} + x_{D_s} \cdot m_{D_s} + x_{E_s} \cdot m_{E_s} - x_{F_s} \cdot m_{F_s} - x_{G_s} \cdot m_{G_s} - \\ & x_{H_s} \cdot m_{H_s} - x_{J_s} \cdot m_{J_s} - x_{K_s} \cdot m_{K_s}) \\ lc_{y_s} =& \frac{1}{m_s}(y_{A_s} \cdot m_{A_s} - y_{B_s} \cdot m_{B_s} - y_{C_s} \cdot m_{C_s} + y_{D_s} \cdot m_{D_s} + y_{E_s} \cdot m_{E_s} - y_{F_s} \cdot m_{F_s} - y_{G_s} \cdot m_{G_s} - \\ & y_{H_s} \cdot m_{H_s} - y_{J_s} \cdot m_{J_s} - y_{K_s} \cdot m_{K_s}) \end{aligned} \tag{44}$$

where the mass center coordinates of each simple geometry represented as $(x_{k_s}, y_{k_s})\ \forall\ k = \{A, B, ..., H, J, K\}$ are given by:

$$\begin{aligned} & x_{A_s} = x_{D_s} = x_{E_s} = \tfrac{l_s + b_s + d_s}{2} - b_s \qquad x_{B_s} = l_s \qquad x_{C_s} = 0 \\ & x_{F_s} = \tfrac{h_s}{3} - b_s \qquad x_{G_s} = l_s + d_s - \tfrac{i_s}{3} \qquad x_{H_s} = \tfrac{j_s}{3} - b_s \\ & x_{J_s} = l_s + d_s - \tfrac{k_s}{3} \qquad y_{A_s} = y_{B_s} = y_{C_s} = 0 \qquad y_{D_s} = \tfrac{f_s + c_s}{2} \\ & y_{E_s} = -\tfrac{g_s + c_s}{2} \qquad y_{F_s} = y_{G_s} = (\tfrac{c_s}{2} + \tfrac{2}{3} f_s) \qquad y_{H_s} = y_{J_s} = (-\tfrac{c_s}{2} - \tfrac{2}{3} g_s) \\ & x_{K_s} = \begin{cases} l'_s \cdot \cos(\hat{\theta}_s) & \text{if } s = 6, 8 \\ 0 & \text{Otherwise} \end{cases} \qquad y_{K_s} = \begin{cases} l'_s \cdot \sin(\hat{\theta}_s) & \text{if } s = 6, 8 \\ 0 & \text{Otherwise} \end{cases} \end{aligned} \tag{45}$$

3.2.3. Inertia

The $s - th$ inertia I_s of the link is shown in (46).

$$I_s = I_{A_s} - I_{B_s} - I_{C_s} + I_{D_s} + I_{E_s} - I_{F_s} - I_{G_s} - I_{H_s} - I_{J_s} - I_{K_s} \tag{46}$$

where the inertia I_{k_s} of the $k - th$ simple geometry $\forall\ k = \{A, B, ..., H, J, K\}$ is defined in (47).

$$\begin{aligned} I_{A_s} =& \tfrac{m_{A_s}}{12}[(l_s + b_s + d_s)^2 + c_s^2] + m_{A_s}[(x_{A_s} - lc_{x_s})^2 + lc_{y_s}^2] \\ I_{B_s} =& \tfrac{m_{B_s}}{2}\tfrac{\phi_s^2}{4} + m_{B_s}[(x_{B_s} - lc_{x_s})^2 + lc_{y_s}^2] \\ I_{C_s} =& \tfrac{m_{B_s}}{2}\tfrac{\phi_s^2}{4} + m_{B_s}(lc_{x_s}^2 + lc_{y_s}^2) \\ I_{D_s} =& \tfrac{m_{D_s}}{12}[(l_s + b_s + d_s)^2 + f_s^2] + m_{D_s}[(x_{D_s} - lc_{x_s})^2 + (y_{D_s} - lc_{y_s})^2] \\ I_{E_s} =& \tfrac{m_{E_s}}{12}[(l_s + b_s + d_s)^2 + g_s^2] + m_{E_s}[(x_{E_s} - lc_{x_s})^2 + (y_{E_s} - lc_{y_s})^2] \\ I_{K_s} =& \begin{cases} \tfrac{m_{B_s}}{2}\tfrac{\phi_s^2}{4} + m_{B_s}[(x_{K_s} - lc_{x_s})^2 + (y_{K_s} - lc_{y_s})^2] & \text{if } s = 6, 8 \\ 0 & \text{Otherwise} \end{cases} \\ I_{F_s} =& \tfrac{m_{F_s}}{18}(h_s^2 + f_s^2) + m_{F_s}[(x_{F_s} - lc_{x_s})^2 + (y_{F_s} - lc_{y_s})^2] \\ I_{G_s} =& \tfrac{m_{G_s}}{18}(i_s^2 + f_s^2) + m_{G_s}[(x_{G_s} - lc_{x_s})^2 + (y_{G_s} - lc_{y_s})^2] \\ I_{H_s} =& \tfrac{m_{H_s}}{18}(j_s^2 + g_s^2) + m_{H_s}[(x_{H_s} - lc_{x_s})^2 + (y_{H_s} - lc_{y_s})^2] \\ I_{J_s} =& \tfrac{m_{J_s}}{18}(k_s^2 + g_s^2) + m_{I_s}[(x_{J_s} - lc_{x_s})^2 + (y_{J_s} - lc_{y_s})^2] \end{aligned} \tag{47}$$

3.3. Constraints

The design constraints are splitted into three groups. The groups are related by the kinematic, dynamic, and shape design. Those are described in the next sections.

3.3.1. Kinematic constraints

The kinematic constraints include the equality constraints given by kinematics of the mechanism (48) and the desired precision points (49); and the inequality constraints provided by the Grashof criterion (50)-(55) and the quality

t_i	$\bar{x}_T$	$\bar{y}_T$	t_i	$\bar{x}_T$	$\bar{y}_T$	t_i	$\bar{x}_T$	$\bar{y}_T$
t_0	0	0	t_7	0.1750	0	t_{14}	0.2591	0.1029
t_1	0.025	0	t_8	0.2	0	t_{15}	0.2094	0.1377
t_2	0.05	0	t_9	0.225	0	t_{16}	0.15	0.15
t_3	0.075	0	t_{10}	0.25	0	t_{17}	0.0906	0.1377
t_4	0.1	0	t_{11}	0.275	0	t_{18}	0.0409	0.1029
t_5	0.125	0	t_{12}	0.3	0	t_{19}	0.009	0.0513
t_6	0.15	0	t_{13}	0.291	0.0513			

Table 1: Twenty desired precision points ($\tilde{N} = 20$) for the human gait in the $(\bar{x}_T, \bar{y}_T)$ coordinate system.

of motion transmission (56)-(61).

The mechanism's kinematic is required to know the (x_E, y_E) coordinate in the mechanism. The desired precision points in the Cartesian coordinate $\bar{X}_T - \bar{Y}_T$ are given in Table 1. Twenty precision points of a semi-ellipse trajectory are considered based on [16] because they represent the main points of interest in the closed trajectory. The continuous closed-trajectory can track a similar semi-ellipse trajectory fulfilling such points. This trajectory represents the physical therapy related to physical exercise to the rehabilitation process. The Grashof constraint ensures that the four-bar mechanism into the rehabilitation one can develop a full crank movement. The quality of motion transmission guarantees the maximum efficiency in the force transmission from the crank link to the (x_E, y_E) point. For more detail about the kinematic constraints (48)-(61), see [16].

$$h_1 = 0 \quad : \quad \begin{bmatrix} x_E(t) \\ y_E(t) \end{bmatrix} - \begin{bmatrix} l_2\cos(\theta_2(t)) + l_3\cos(\theta_3(t)) + l'_8\cos(\theta_8(t)+\hat{\theta}_8) \\ l_2\sin(\theta_2(t)) + l_3\sin(\theta_3(t)) + l'_8\sin(\theta_8(t)+\hat{\theta}_8) \end{bmatrix} = \begin{bmatrix} 0 \\ 0 \end{bmatrix} \tag{48}$$

$$h_2 = 0 \quad : \quad [\bar{x}_E(t), \bar{y}_E(t)] - [x_{ini}, y_{ini}] - [x_T(t), y_T(t)] = [0,0] \tag{49}$$

$$g_1 \leq 0 \quad : \quad l_2 + l_1 - l_3 - l_4 \leq 0 \tag{50}$$

$$g_2 \leq 0 \quad : \quad -l_4 - l_1 + l_2 + l_3 \leq 0 \tag{51}$$

$$g_3 \leq 0 \quad : \quad -l_3 - l_1 + l_2 + l_4 \leq 0 \tag{52}$$

$$g_4 \leq 0 \quad : \quad l_2 + l_9 - l_3 - l'_6 \leq 0 \tag{53}$$

$$g_5 \leq 0 \quad : \quad -l'_6 - l_9 + l_2 + l_3 \leq 0 \tag{54}$$

$$g_6 \leq 0 \quad : \quad -l_3 - l_9 + l_2 + l'_6 \leq 0 \tag{55}$$

$$g_7 \leq 0 \quad : \quad \frac{\pi}{4} - \cos^{-1}\left(\frac{l_3^2 + l_4^2 - (l_1 - l_2)^2}{2l_3l_4}\right) \leq 0 \tag{56}$$

$$g_8 \leq 0 \quad : \quad \frac{\pi}{4} - \cos^{-1}\left(\frac{l_5^2 + {l'_6}^2 - (l_9 - l_2)^2}{2l_5l'_6}\right) \leq 0 \tag{57}$$

$$g_9 \leq 0 \quad : \quad \cos^{-1}\left(\frac{l_3^2 + l_4^2 - (l_1 + l_2)^2}{2l_3l_4}\right) - \frac{3\pi}{4} \leq 0 \tag{58}$$

$$g_{10} \leq 0 \quad : \quad \cos^{-1}\left(\frac{l_5^2 + {l'_6}^2 - (l_9 + l_2)^2}{2l_5l'_6}\right) - \frac{3\pi}{4} \leq 0 \tag{59}$$

$$g_{11} \leq 0 \quad : \quad \theta_8(t) - \theta_7(t) + 2\pi - \frac{3\pi}{4} \leq 0 \tag{60}$$

$$g_{12} \leq 0 \quad : \quad \frac{\pi}{4} - \theta_8(t) - \theta_7(t) + 2\pi \leq 0 \tag{61}$$

3.3.2. Dynamic constraints

The Inverse Dynamic Model (IDM) of the rehabilitation mechanism and mechanical failure prevention in joints conform the dynamic constraints.

The IDM computes the input torque generated in the crank link and also forces in joints of the rehabilitation mechanism required to track the precision points with the external force $\vec{F}_{K_8}$ exerted in the (x_E, y_E) mechanism coordinate. Then, the IDM is included as equality constraints (62).

$$h_3 : \check{X} - \check{A}(p)^{-1}\check{B}(p) = 0 \tag{62}$$

The other important dynamic constraint is related to the maximum applied forces supported by link joints. Those joints are more prone to get a mechanical failure, i.e., the maximum stress is presented in those areas. Let the $s-th$ contact area $a_s = \frac{\pi}{4}\phi_s e_s$ of the joint forces and the $\hat{k}-th$ contact stress in the $s-th$ contact area $\sigma_{\hat{k}_s} = \frac{||\vec{F}_{\hat{k}_s}||}{a_s}$, then the safety factor for each joint must be larger or at least equal than the design factor $Fc_{min} = 1.5$. Therefore, the inequality constraint (63) related to avoiding the mechanical failure in joints is incorporated, where the permissible

stress $\sigma_{adm} = 6.2052 \times 10^7 Pa$ of the aluminum is related to the elastic limit.

$$g_{13} \leq 0 : Fc_{min} - \frac{\sigma_{adm}}{\sigma_{\hat{k}_s}} \leq 0 \; \forall \; \hat{k} = \{B, C, K\} \; \wedge \; s = \{2, 3, ..., 8\} \tag{63}$$

3.3.3. Link shape constraints

The first link shape constraints (64)-(65) keeps the octagonal prism shape.

$$g_{14} \leq 0 \quad : \quad h_s + i_s - b_s - l_s - d_s \leq 0 \; \forall \; s = \{2, 3, ..., 8\} \tag{64}$$

$$g_{15} \leq 0 \quad : \quad j_s + k_s - b_s - l_s - d_s \leq 0 \; \forall \; s = \{2, 3, ..., 8\} \tag{65}$$

The second constraints avoid the overlapping of the K_s, C_s and B_s holes. This is represented by (66)-(68). In this case, the minimum distance between hole edges is chosen as $\psi_s = 1.5\phi_s$ to prevent tearing fail.

$$g_{16} \leq 0 \quad : \quad \psi_s - l_s + \phi_s \leq 0 \; \forall \; s = \{2, 3, ..., 8\} \tag{66}$$

$$g_{17} \leq 0 \quad : \quad \psi_s - \sqrt{x_{K_s}^2 + y_{K_s}^2} + \phi_s \leq 0 \; \forall \; s = \{6, 8\} \tag{67}$$

$$g_{18} \leq 0 \quad : \quad \psi_s - \sqrt{(x_{K_s} - x_{B_s})^2 + (y_{K_s} - y_{B_s})^2} + \phi_s \leq 0 \; \forall \; s = \{6, 8\} \tag{68}$$

The third constraints determine if the K_s, C_s and B_s holes are inside of the octagonal area i.e, set a minimal distance from the hole to the collinear lines $z_i = 0 \; \forall \; i = \{1, 2, ..., 8\}$ of the link edges. This is represented by (69)-(76). The collinear lines can be expressed as $\bar{A}x_{\hat{k}_s} + \bar{B}y_{\hat{k}_s} + \bar{C} = 0$, where the coordinate $(x_{\hat{k}_s}, y_{\hat{k}_s})$ is with respect to the frame $x_s - y_s$ in the octagonal link (see Fig. 2) and the terms $\bar{A}$, $\bar{B}$ and $\bar{C}$ are the polynomial coefficients. Given the coordinate $(x_{\hat{k}_s}, y_{\hat{k}_s}) \; \forall \; \hat{k} = \{K, C, B\}$ as the hole center and considering that $z_i \leq 0 \; \forall \; i = \{1, 2, ..., 8\}$, the $\hat{k} - th$ hole center of the $s - th$ link must be in the Hole Feasible Region (HFR), see Fig. 2. Then, the perpendicular distance from the hole center point to the corresponding collinear line $z_i = 0$ of the link edges must be smaller than $\bar{D} = -\zeta_s - \frac{\phi_s}{2}$ i.e., $\frac{\bar{A} \cdot x_{\hat{k}_s} + \bar{B} \cdot y_{\hat{k}_s} + \bar{C}}{\sqrt{\bar{A}^2 + \bar{B}^2}} \leq \bar{D}$ to guarantee that the complete hole is in HFR. The term $\zeta_s = 1.5\phi_s$ is established as the distance between the hole edge and the octagonal edge to avoid tearing fail.

$$g_{19} \leq 0 \quad : \quad \overbrace{-y_{\hat{k}_s} - \frac{c_s}{2} - g_s}^{z_1} + \zeta_s + \frac{\phi_s}{2} \leq 0 \tag{69}$$

$$g_{20} \leq 0 \quad : \quad \frac{\overbrace{-y_{\hat{k}_s} - \frac{g_s}{j_s} \cdot x_{\hat{k}_s} - \frac{c_s}{2} + \frac{g_s \cdot b_s}{j_s}}^{z_2}}{\sqrt{\frac{g_s}{j_s}^2 + 1}} + \zeta_s + \frac{\phi_s}{2} \leq 0 \tag{70}$$

$$g_{21} \leq 0 \quad : \quad \overbrace{-x_{\hat{k}_s} - b_s}^{z_3} + \zeta_s + \frac{\phi_s}{2} \leq 0 \tag{71}$$

$$g_{22} \leq 0 \quad : \quad \frac{\overbrace{y_{\hat{k}_s} - \frac{f_s}{h_s} \cdot x_{\hat{k}_s} - \frac{c_s}{2} - \frac{f_s \cdot b_s}{h_s}}^{z_4}}{\sqrt{\frac{f_s}{h_s}^2 + 1}} + \zeta_s + \frac{\phi_s}{2} \leq 0 \tag{72}$$

$$g_{23} \leq 0 \quad : \quad \overbrace{y_{\hat{k}_s} - \frac{c_s}{2} - f_s}^{z_5} + \zeta_s + \frac{\phi_s}{2} \leq 0 \tag{73}$$

$$g_{24} \leq 0 \quad : \quad \frac{\overbrace{y_{\hat{k}_s} + \frac{f_s}{i_s} \cdot x_{\hat{k}_s} - \frac{c_s}{2} - \frac{f_s \cdot (a_s + d_s)}{i_s}}^{z_6}}{\sqrt{\frac{f_s}{i_s}^2 + 1}} + \zeta_s + \frac{\phi_s}{2} \leq 0 \tag{74}$$

$$g_{25} \leq 0 \quad : \quad \overbrace{x_{\hat{k}_s} - a_s - d_s}^{z_7} + \zeta_s + \frac{\phi_s}{2} \leq 0 \tag{75}$$

$$g_{26} \leq 0 \quad : \quad \frac{\overbrace{-y_{\hat{k}_s} - \frac{g_s}{k_s} \cdot x_{\hat{k}_s} - \frac{c_s}{2} - \frac{g_s \cdot (a_s + d_s)}{k_s}}^{z_8}}{\sqrt{\frac{g_s}{k_s}^2 + 1}} + \zeta_s + \frac{\phi_s}{2} \leq 0 \tag{76}$$

3.3.4. Design variable bounds

The last constraints associate the bounds in the design variables $p \in R^{87+\tilde{N}}$ to limit the search for the solution. In (77), those bounds are established as inequality constraints, where p_{min} and p_{max} are the minima and maximum design variable values, and those are presented in Table 2.

$$p_{min} \leq p \leq p_{max} \tag{77}$$

3.3.5. Optimization problem statement

The optimization problem consists of finding the kinematic and shape design variable grouped in $p \in R^{87+\tilde{N}}$ that minimize the precision point tracking error $\bar{J}_1$ and the energy consumption $\bar{J}_2$ subject to the bounds in p, the kinematic, the dynamic, and the link shape constraints. This multi-objective optimization problem is formulated as a mono-objective one with the weighted sum approach as is shown in (78)-(81). The desired trade-off is selected through the weights $\kappa_1 = 1$ and $\kappa_2 = 1 \times 10^{-6}$. These weights are chosen by a series of trial and error procedures.

$$\begin{aligned} &\underset{p}{\text{Min}} && J = \kappa_1 \cdot \bar{J}_1 + \kappa_2 \cdot \bar{J}_2 \\ &\text{subject to:} \\ & && g(p) \ \leq \ 0 \qquad (79) \\ & && h(p) = 0 \qquad (80) \\ & && p_{Min} \leq \ p \leq p_{Max} \qquad (81) \end{aligned} \tag{78}$$

4. Differential evolution algorithm

The Differential Evolution (DE) algorithm is used to solve the optimization problem. This is classified as an Evolutionary Algorithm (EA), and it is a stochastic search method. The algorithm was proposed in 1995 by R. Storn y K. V. Price [18]. DE has been used in diverse applications in mechanical engineering, communications, and pattern recognition. The operating principle of DE is the natural evolution and survival of the fittest to search for better solutions in each generation through three basic operators of the evolutionary process: mutation, crossover, and selection. These operators allow exploring/exploiting the search space to find a region near the global solution and hence, avoid local solutions. DE has been used to solve engineering problems and gained more attention in the

Algorithm 1 Pseudo-code of the differential evolution variants $DE/a/b/c$.

```
Generate initial population X_0 with NP individuals.
Evaluate X_0
G ← 0
while G ≤ G_max do
   for each x_i ∈ X_G do
      Generate a child individual u_i based on (82)-(89)
      Evaluate u_i
   end for
   Select individuals for G + 1 according to CHC
   G ← G + 1
end while
```

synthesis of mechanisms [19, 20]. This is because they provide good approximate solutions, are less likely to get stuck at local minima, and are not sensitive to initial conditions; they are free derivative, and also they can endow, in an easy way, outstanding features of other algorithms to make a better exploration and exploitation in the solution search. Nevertheless, the DE algorithm and all EAs require several tests to verify the reliability of the obtained solution. For instance, at [21] the authors showed that DE performs better than Particle Swarm Optimization (PSO) and Genetic Algorithms (GA) for the synthesis of four-bar mechanisms.

In this work, eight variants of differential evolution are considered. Each variant is different by the crossover and mutation process. The most popular nomenclature for the variants is referred to as $DE/a/b/c$, where DE means differential evolution, a indicates the individual's selection for the mutation stage, b is the number of pairs of solutions, and c means the type of recombination.

Algorithm 1 shows the DE pseudo-code. The process starts with an initial population X_0 called parents with NP randomly generated individuals in the search space. The parents mutate and recombine through each generation G by using (82) - (89) to generate the child population. The mutation rate F is randomly selected per generation in the range $[0.3, 0.9]$, CR is the crossover rate and the superscript $r_i \; \forall \; i = \{1, 2, 3\}$ and $best$ indicate the random and the best individuals obtained from the parent population. The child and parent population compete between them to preserve the aptest in the next generation. The synergy between the precision in the point tracking and the energy consumption must be considered in the optimization problem formulation and an important factor to be analyzed in the Concurrent Design is the search for solutions that promote a better design trade-off. As the No Free Lunch Theorem states [22] that an algorithm would perform well on a certain class of problems, but it could not be true for the remaining problems, then it is necessary to use different optimization techniques to find the most suitable solution in the particular optimization

Kinematic parameters $\tilde{p}_{ki}$	p_{min}	p_{max}
p_1-p_{11}	0	0.75
p_{12}-p_{15}, p_{18}-p_{37}	0	2π
p_{16}	-1.875	1.875
p_{17}	-1.875	-0.15
Shape parameters $\tilde{p}_{sh}$		
p_{38}-p_{41}, p_{43}, p_{45}-p_{48}, p_{50}, p_{66}-p_{69}, p_{71}, p_{73}-p_{76}, p_{78}	0	0.1
p_{42}, p_{44}, p_{49}, p_{51}, p_{56}, p_{58}, p_{70}, p_{72}, p_{77}, p_{79}	0	0.5

Shape parameters $\tilde{p}_{sh}$	p_{min}	p_{max}
p_{52}	0	0.3
p_{53}-p_{55}, p_{57}	0	0.15
p_{59}-p_{65}	0.01	0.05
p_{80}-p_{107}	0	1.875

Table 2: Maximum and minimum design parameters vector p.

problem. Eight different DE variants are considered to promote further exploration and exploitation of the search space and hence, promote different synergy (reconfigurability) in the lower limb rehabilitation mechanism. Those variants are chosen according to the kind of recombination operator and the individuals' selection in the mutation process. Four variants present binomial and exponential discrete recombination. Those are: $Rand/1/Bin$ (DER1B), $Best/1/Bin$ (DEB1B), $Rand/1/Exp$ (DER1BE) and $Best/1/Exp$ (DEB1E). Two variants includes arithmetic recombination such as $Current-to-Rand/1$ (DECR1) and $Current-to-Best/1$ (DECB1). The last two variants have hybrid operators between the arithmetic and the discrete recombination. Those are: $Current-to-Rand/1/Bin$ (DECR1B) and $Current-to-Rand/1/Exp$ (DECR1E).

Binomial discrete recombination:

$$Rand/1/Bin: u_j^i = \begin{cases} v_j^i = x_j^{r_3} + F(x_j^{r_1} - x_j^{r_2}), & \text{if } rand_j(0,1) < CR \text{ or } j = j_{rand} \\ x_j^i, & \text{Otherwise} \end{cases} \tag{82}$$

$$Best/1/Bin: u_j^i = \begin{cases} v_j^i = x_j^{best} + F(x_j^{r_1} - x_j^{r_2}), & \text{if } rand_j(0,1) < CR \text{ or } j = j_{rand} \\ x_j^i & \text{Otherwise} \end{cases} \tag{83}$$

$$Rand/1/Exp: u_j^i = \begin{cases} v_j^i = x_j^{r_3} + F(x_j^{r_1} - x_j^{r_2}), & \text{from } rand_j(0,1) < CR \text{ or } j = j_{rand} \\ x_j^i, & \text{Otherwise} \end{cases} \tag{84}$$

$$Best/1/Exp: u_j^i = \begin{cases} v_j^i = x_j^{best} + F(x_j^{r_1} - x_j^{r_2}), & \text{from } rand_j(0,1) < CR \text{ or } j = j_{rand} \\ x_j^i & \text{Otherwise} \end{cases} \tag{85}$$

Arithmetic recombination:

$$Current-to-Rand/1: \vec{u}^i = v_j^i = \vec{x}^i + K(\vec{x}^{r_3} - \vec{x}^i) + F(\vec{x}^{r_1} - \vec{x}^{r_2}) \tag{86}$$

$$Current-to-Best/1: \vec{u}^i = v_j^i = \vec{x}^i + K(\vec{x}^{best} - \vec{x}^i) + F(\vec{x}^{r_1} - \vec{x}^{r_2}) \tag{87}$$

Arithmetic-discrete recombination:

$$Current-to-Rand/1/Bin: u_j^i = \begin{cases} u_j^i = x_j^i + K(x_j^{r_3} - x_j^i) + F(x_j^{r_1} - x_j^{r_2}) & \text{if } rand_j(0,1) < CR \text{ or } j = j_{rand} \\ x_j^i & \text{Otherwise} \end{cases} \tag{88}$$

$$Current-to-Rand/1/Exp: u_j^i = \begin{cases} u_j^i = x_j^i + K(x_j^{r_3} - x_j^i) + F(x_j^{r_1} - x_j^{r_2}) & \text{from } rand_j(0,1) < CR \text{ or } j = j_{rand} \\ x_j^i & \text{Otherwise} \end{cases} \tag{89}$$

On the other hand, the selection process between the child and the parent population is based on the following statement [23]:

1. A feasible individual is chosen over an infeasible one.
2. Between two feasible individuals, the one with a higher fitness is chosen.
3. Between two Infeasible Individuals (InfInd), the one with the lowest constraint distance is chosen i.e., $\sum_i^m max(0, g_i)$.
4. Between two Infeasible Individuals with the same constraint distance, the individual is chosen by a random selection.

Unlike what was reported in [23], the penalization of the infeasible individuals is taken with respect to the sum of the constraint value instead of the number of violated constraints. Based on a series of empirical experiments, this

Algorithm	Mean	Standard deviation	Median	Best	Worst
DER1B	**0.0007609**	0.000434	**0.0008604**	$\mathbf{1.958 \times 10^{-5}}$	0.001476
DER1E	0.00251	0.0003648	0.002448	6.797×10^{-5}	0.04095
DEB1B	0.001139	0.0008696	0.001023	4.14×10^{-5}	0.00446
DEB1E	0.002997	0.00109	0.002818	6.369×10^{-5}	0.2768
DECR	0.001183	0.00053	0.00126	4.747×10^{-5}	0.07003
DECB	0.002226	0.002894	0.001444	18.34×10^{-5}	0.6288
DECR1B	0.0008602	**0.0004145**	0.0009596	7.493×10^{-5}	0.01917
DECR1E	0.002421	0.0003408	0.002352	$8.866e \times 10^{-5}$	0.03839

Table 3: Descriptive statistic of the DE variant executions.

promotes an efficient search in the mechanism synthesis of the lower limb rehabilitation mechanism.

5. Results

This section involves the performance analysis in the optimization algorithm to find the most suitable synergy in the Concurrent Design for the lower limb rehabilitation mechanism and also, obtain the design for carrying out the repetitive gait movement with less energy consumption. Besides, the comparative analysis of the proposed Concurrent Design approach with respect to a mechanism designed with a traditional design approach is carried out.

5.1. Algorithm performance analysis for finding the optimum solution

Thirty independent executions for each of the eight DE variants are developed in C programming language by using a personal computer with AMD A8-7410 APU @ 2.20 GHz processor and 12GB of RAM. The algorithm parameters are set as follows: Sixty individuals into the population, i.e., $NP = 60$ with a maximum generation number of $G_{max} = 200000$. The crossover rate is chosen as $CR = 0.9$, and the scale factor F and the parameter K are randomly selected in the interval $[0.3, 0.9]$.

In each execution, the average value of the objective functions of individuals in the last generation is stored, and the data for all executions are analyzed by using the descriptive statistic shown in Table 3. According to this table, the Rand/1/Bin variant of the differential evolution algorithm (DER1B) presents the smallest mean value and finds the minimum value of the objective function through executions (the best design solution in the optimization problem) with respect to the other DE variants. Hence, the DER1B variant provides an efficient exploration and exploitation in search of a solution. Hence, it promotes the best synergy (reconfigurability) in the design of the lower limb rehabilitation mechanism.

The behavior of the objective functions for the best solution per each DE variant is displayed in Fig. 3. This empirically confirms that exponential discrete recombination in DECR1E, DER1E, and DEB1E variants increases the exploration of the search space due to the objective functions becoming settled around sixty percent of the total generations. Meanwhile, the use of binomial discrete recombination (DEB1B, DECR1B) and the arithmetic ones (DECR,DECB) enhance the exploitation of the search space because the objective functions become settled around the five percent of the total generations. Increasing only the exploration or the exploitation of the search space results in local optimum solutions. So, the best performance is obtained by the DER1B. This is attributed because it can

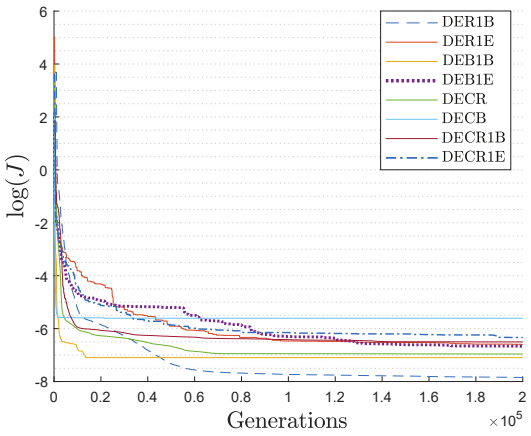

Figure 3: Objective function convergence of the best solution per each DE variant.

Kinematic parameters $\tilde{p}^*_{ki}$													
P_1	P_2	P_3	P_4	P_5	P_6	P_7	P_8	P_9	P_{10}	P_{11}	P_{12}	P_{13}	P_{14}
0.5981	0.1397	0.7102	0.6402	0.5136	0.5560	0.5779	0.5673	0.6601	0.3047	0.3115	1.8190	2.6483	5.2237
P_{15}	P_{16}	P_{17}	P_{18}	P_{19}	P_{20}	P_{21}	P_{22}	P_{23}	P_{24}	P_{25}	P_{26}	P_{27}	P_{28}
0.1413	-0.4954	-0.3949	3.1571	2.9244	2.7350	2.5770	2.4377	2.3019	2.1657	2.0208	1.8622	1.6834	1.4707
P_{29}	P_{30}	P_{31}	P_{32}	P_{33}	P_{34}	P_{35}	P_{36}	P_{37}					
1.1568	0.7969	0.2187	5.9403	5.4842	5.0356	4.5801	4.1582	3.7168					
Shape parameters $\tilde{p}^*_{sh}$													
P_{38}	P_{39}	P_{40}	P_{41}	P_{42}	P_{43}	P_{44}	P_{45}	P_{46}	P_{47}	P_{48}	P_{49}	P_{50}	P_{51}
0.3000	0.2998	0.0772	0.0896	0.2082	0.3000	0.4960	0.1000	0.0763	0.0760	0.0992	0.1132	0.0762	0.0692
P_{52}	P_{53}	P_{54}	P_{55}	P_{56}	P_{57}	P_{58}	P_{59}	P_{60}	P_{61}	P_{62}	P_{63}	P_{64}	P_{65}
0.0381	0.0383	0.0383	0.0382	0.0382	0.0382	0.0382	0.0500	0.0100	0.0100	0.0499	0.0100	0.0100	0.0100
P_{66}	P_{67}	P_{68}	P_{69}	P_{70}	P_{71}	P_{72}	P_{73}	P_{74}	P_{75}	P_{76}	P_{77}	P_{78}	P_{79}
0.1000	0.0001	0.0005	0.0000	0.0007	0.0000	0.0475	0.0999	0.0002	0.0997	0.1000	0.2476	0.1000	0.0035
P_{80}	P_{81}	P_{82}	P_{83}	P_{84}	P_{85}	P_{86}	P_{87}	P_{88}	P_{89}	P_{90}	P_{91}	P_{92}	P_{93}
0.0000	0.0332	0.1977	0.2928	0.3097	0.1261	0.8049	0.1596	0.9101	0.1801	0.3411	0.3606	0.1246	0.2941
P_{94}	P_{95}	P_{96}	P_{97}	P_{98}	P_{99}	P_{100}	P_{101}	P_{102}	P_{103}	P_{104}	P_{105}	P_{106}	P_{107}
0.0006	0.0063	0.0020	0.0002	0.3454	0.0001	0.3445	0.3939	1.0123	0.4199	0.0002	0.4354	0.8256	0.0340

Table 4: Optimum design variable vector $p^* = [\tilde{p}_{ki}, \tilde{p}_{sh}]^T$ obtained by the Concurrent Design approach.

efficiently balance the trade-off between the exploration and exploitation processes in search of the solution such that better reconfigurability in the rehabilitation mechanism design is achieved.

5.2. Performance analysis in the obtained design for the rehabilitation mechanism.

According to the descriptive statistics given in Table 3, the best design solution p^* obtained by DER1B is shown in Table 4. This has an objective function of $J^* = 1.958 \times 10^{-5}$. The link shapes are presented in Fig. 4. The performance in the precision point tracking is introduced in Fig. 5 where the precision point tracking error is $\bar{J}_1^* = 1.53 \times 10^{-5}\ m^2$ which provides a maximum and minimum Euclidean distance between the desired and generated precision points of $9 \times 10^{-3}\ m$ and $9.68 \times 10^{-5}\ m$, respectively. In addition, the total applied torque is $\bar{J}_2^* = 4.18\ N^2m^2$. It is important to remark that the obtained solution fulfills the design constraints given in Section 3.

On the other hand, a Finite Element Analysis (FEA) is carried out for each link to get the von Mises stress. The Matlab® software and the PDE Modeler Tool are used to perform the two-dimensional FEA. The numerical simulation of the inverse dynamic analysis is carried out to obtain the maximum magnitude of the joint force. For this analysis an integration step of $1ms$ with a maximum crank speed of $\omega_2 = 2\pi\ rad/s$ are taken into account for a complete cycle of the rehabilitation mechanism (full rotation of the mechanism crank). With the maximum force information and with

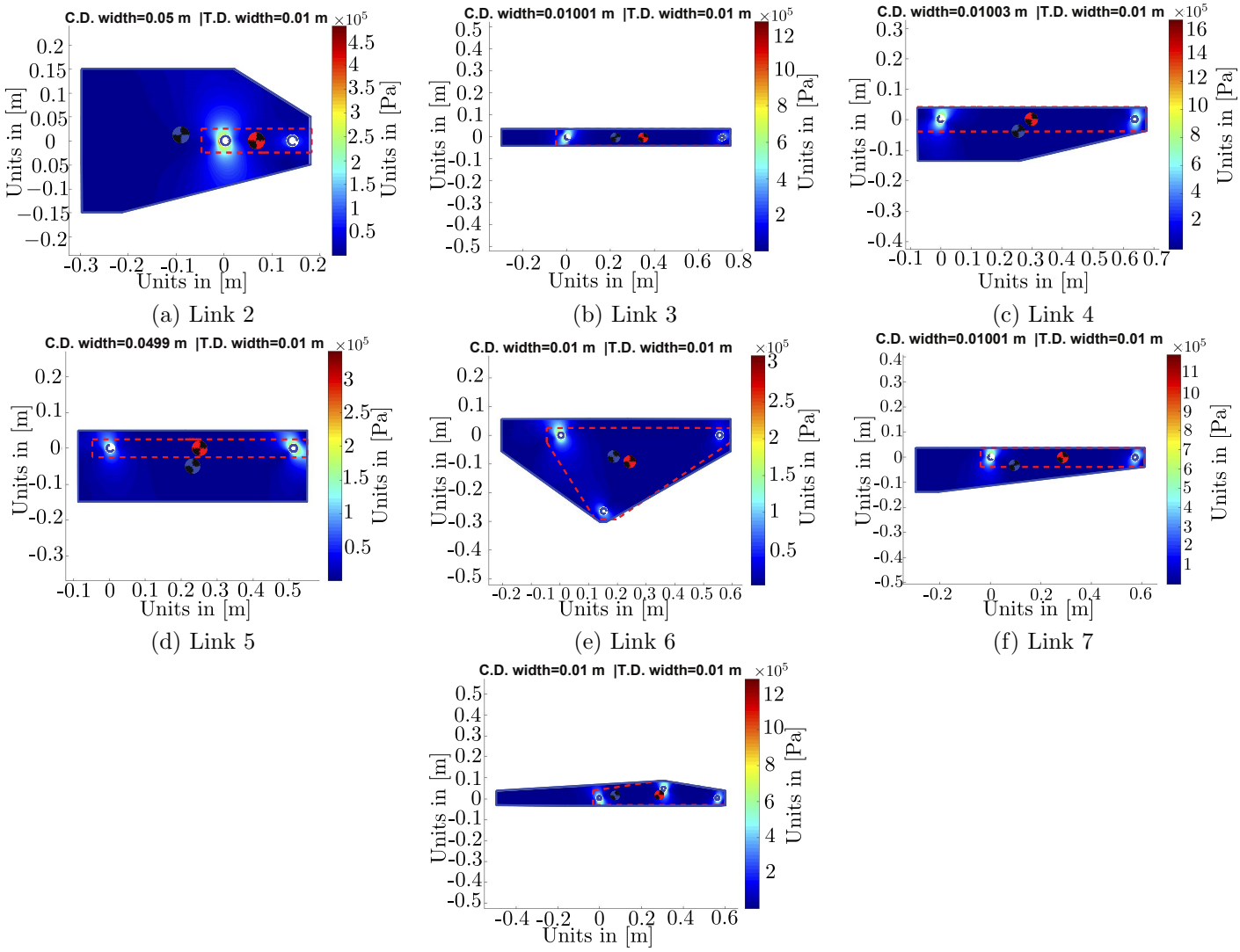

(a) Link 2 (b) Link 3 (c) Link 4

(d) Link 5 (e) Link 6 (f) Link 7

(g) Link 8

Figure 4: Link shapes of the optimal solution. Continuous line and dashed line represent the obtained solution by the proposed Concurrent Design (C.D.) approach and by the Traditional Design (T.D.) approach, respectively. The maximum von Mises stress of links in the Concurrent Design is also visualized.

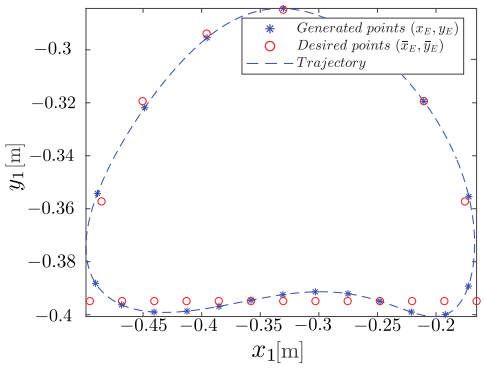

Figure 5: Behavior of the precision point tracking with the best design p^*.

Link	2	3	4	5	6	7	8
$\sigma_{vM}[Pa]$	4.8327×10^5	1.2631×10^6	1.6388×10^6	3.4113×10^5	3.1355×10^6	1.1951×10^6	1.2848×10^6

Table 5: Von Mises maximum stress through the full rotation of the crank.

the maximum applied force $\vec{F}_{K_8} = [0, -133.41]^T$ N in the point (x_E, y_E) related to the lower limb weight, the FEA analysis can be done.

The von Mises stress σ_{vM} for each link is shown in Fig.4 where the maximum values are presented in Table 5 . As can be observed, the maximum von Mises stress in the links does not overcome the permissible stress $\sigma_{adm} = 62052815.64\ Pa$ of the link material (aluminum). Hence, the rehabilitation mechanism cannot present permanent deformation in the links with the maximum mass of the Mexican population lower limb, i.e., the link material does not yield with such a force.

5.3. Biomechanical analysis of the rehabilitation machine

The Computer-Aided Design (CAD) of the obtained rehabilitation mechanism with the best-found design (p^*) is displayed in Fig. 6. The position of the seat is a key factor for guaranteeing that the rehabilitation machine allows the natural movement of the lower limb and avoids joint mobility problems. Considering that the maximum and minimum reported human height H of the Mexican population is $H = 1.90\ m$ and $H = 1.63\ m$, respectively [17], and employing the anthropometric analysis [24] to compute the corresponding thigh and leg lengths, the seat position coordinate (x_A, y_A) can be obtained from the origin $x_1 - y_1$ as $x_A = 0.5589H - 0.6959\ m$ and $y_A = -0.1318\ m$. For more details of the procedure to obtain the seat coordinates ($[x_A, y_A]$), see (S59)-(S63) of the Supplementary Material.

The biomechanical analysis of the rehabilitation machine consists of testing the movement of the lower limb. When the foot is tied to the Cartesian point $[x_E, y_E]$ of the mechanism, we must guarantee that the rehabilitation machine allows the lower limb's natural movement to avoid joint mobility problems. In this case, the coxofemoral joint angle ξ and the knee joint angle φ for the full rotation of the crank is presented in Fig. 7. These joint angles are obtained by developing the numerical simulation of the lower limb movement in Solidworks® using the maximum (1.90 m), and minimum (1.63 m) reported height of the Mexican population [17]. The corresponding thigh-length $L_t = 0.53H - 0.285H$ and leg ones $L_l = 0.285H - 0.039H$ in the numerical simulation are computed by employing the

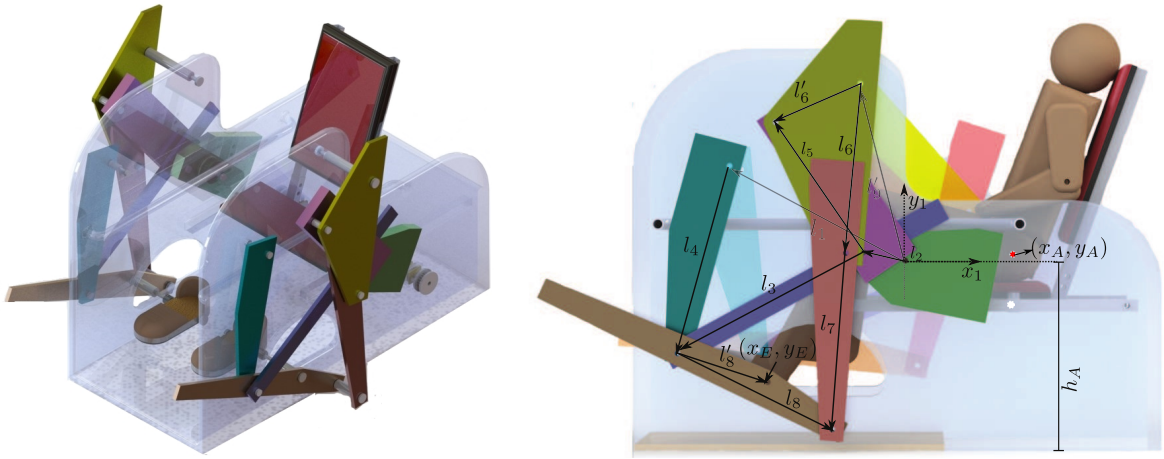

(a) (b)

Figure 6: The CAD of the obtained eight-bar mechanism for the rehabilitation machine.

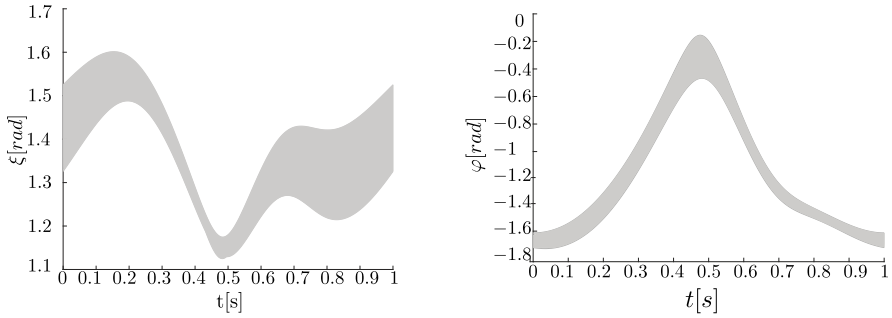

(a) Coxofemoral joint movement ξ. (b) Knee joint movement φ.

Figure 7: Lower limb joint behavior considering a full crank rotation of the eight-bar mechanism with the maximum and minimum height of the Mexican population.

anthropometric analysis in [24], where H is the human height. For illustrative purpose, a CAD representation of the lower limb movement in the rehabilitation machine for the Mexican population's average height is presented in Fig. 8.

Based on Fig. 7, it is confirmed that the joint angles are into the permitted lower limb natural movement [25]. For the particular case of the Mexican population, the coxofemoral and knee joint movements are into the interval $[-0.34, 2.09]$ *rad* and $[-2.26, 0]$ *rad*. Hence, the proposed mechanism can safely develop the predefined rehabilitation routine.

Finally, the prototype of the 1:6 scale modeling of the rehabilitation machine is manufactured with a three-dimensional (3D) printer, and this is illustrated in Fig. 9. A video showing the rehabilitation mechanism's movement with the proposed concurrent design approach is given in the following link : *www.dropbox.com/s/g2blg2dgsii91et/Proyecto.mp4?dl=*

5.4. Comparative analysis

To show the advantages of the proposed Concurrent Design (C.D.) in the rehabilitation mechanism, comparative results between the design obtained by the proposal and the design achieved by using a Traditional Design (T.D.)

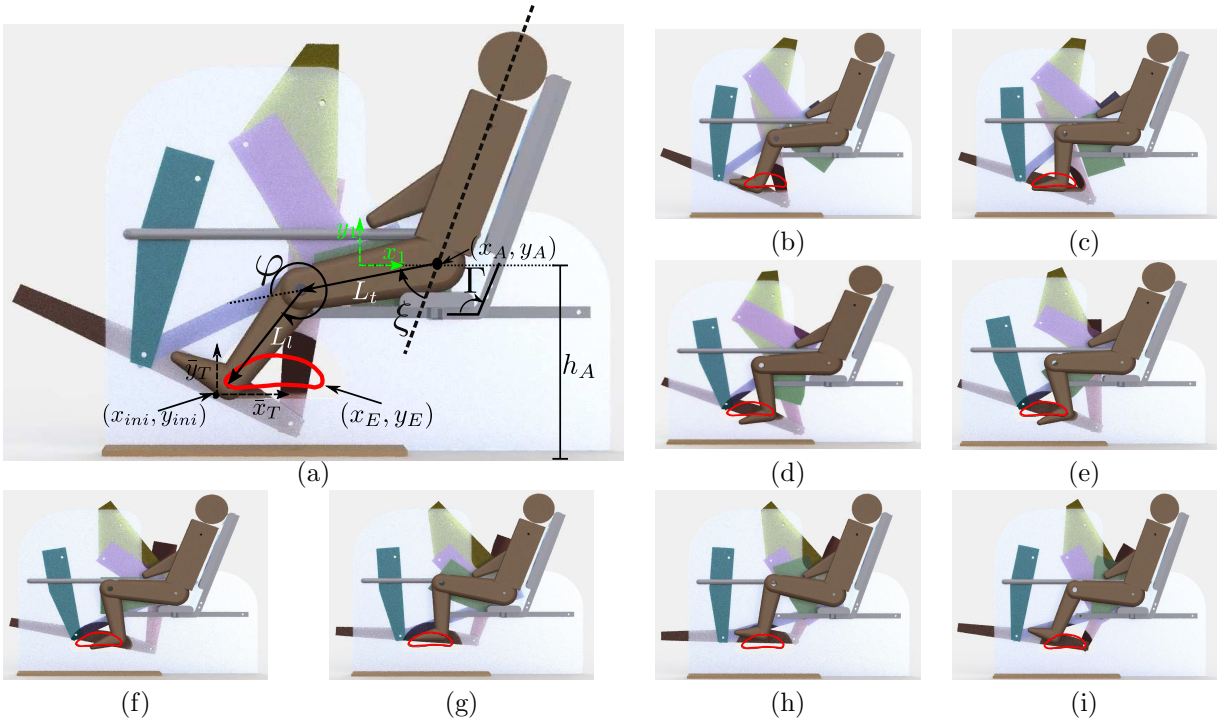

Figure 8: Graphical representation of rehabilitation machine through a crank full-rotation.

approach is carried out. The traditional design involves the optimum kinematic synthesis of the rehabilitation mecha-
305 nism where the design variable vector $p^{Tra} \in R^{17+\tilde{N}}$ is only related to the kinematic parameter vector $\tilde{p}_{ki}$ (the shape parameters are not considered). In this case, the optimum traditional design is accomplished with the optimum kinematic parameters obtained by the concurrent design, i.e., $p^{*Tra} = \tilde{p}^*_{ki}$. The link shape parameters of the T.D. consider rectangular and triangular shapes with the link width of 0.01 m (see dashed line links in Fig. 4). The link dynamic parameters for both designs are included in Table 6. The total mass of links in the concurrent design is 49.04 Kg, whilst
310 the ones related to the traditional design is 11.63 Kg. An increment of 422% of the total mass of links is provided by the concurrent design with respect to the traditional design. The CAD of the rehabilitation mechanisms with both designs is displayed in Fig. 10.

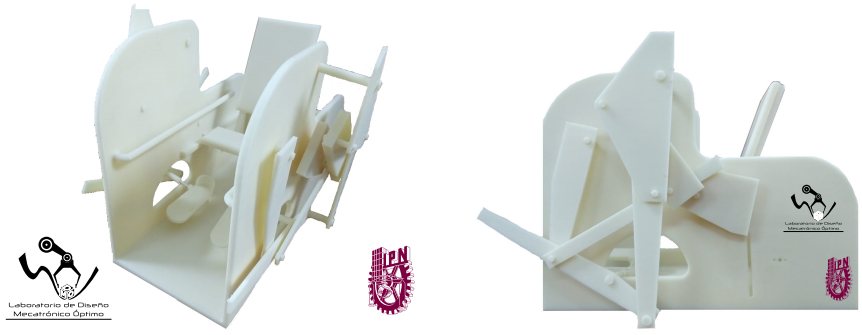

(a) Isometric view. (b) Lateral view.

Figure 9: Scale modeling prototype of the rehabilitation mechanism.

m_2 [kg]	m_3 [kg]	m_4 [kg]	m_5 [kg]	m_6 [kg]	m_7 [kg]	m_8 [kg]
C.D. | T.D.	C.D. | T.D.	C.D. | T.D.	C.D. | T.D.	C.D. | T.D.	C.D. | T.D.	C.D. | T.D.
15.5292 | 0.2921	2.1218 | 1.6086	3.0092 | 1.6316	17.1338 | 1.7025	5.1925 | 3.4725	3.2289 | 1.3349	2.8290 | 1.5854
I_2 [$kg\ m^2$]	I_3 [$kg\ m^2$]	I_4 [$kg\ m^2$]	I_5 [$kg\ m^2$]	I_6 [$kg\ m^2$]	I_7 [$kg\ m^2$]	I_8 [$kg\ m^2$]
C.D. | T.D.	C.D. | T.D.	C.D. | T.D.	C.D. | T.D.	C.D. | T.D.	C.D. | T.D.	C.D. | T.D.
0.3478 | 0.0013	0.1898 | 0.0824	0.1323 | 0.0776	0.6414 | 0.0593	0.2432 | 0.1009	0.2168 | 0.0478	0.2570 | 0.0471
lc_{2_x} [m]	lc_{3_x} [m]	lc_{4_x} [m]	lc_{5_x} [m]	lc_{6_x} [m]	lc_{7_x} [m]	lc_{8_x} [m]
C.D. | T.D.	C.D. | T.D.	C.D. | T.D.	C.D. | T.D.	C.D. | T.D.	C.D. | T.D.	C.D. | T.D.
-0.1381 | -0.2951	-0.1787 | -0.0672	0.3484 | 0.3024	-0.2129 | -0.1841	-0.1305 | -0.1486	-0.3598 | -0.3573	0.1708 | -0.0375
lc_{2_y} [m]	lc_{3_y} [m]	lc_{4_y} [m]	lc_{5_y} [m]	lc_{6_y} [m]	lc_{7_y} [m]	lc_{8_y} [m]
C.D. | T.D.	C.D. | T.D.	C.D. | T.D.	C.D. | T.D.	C.D. | T.D.	C.D. | T.D.	C.D. | T.D.
0.0103 | 0.0011	-0.0974 | -0.1556	0.0533 | 0.0168	0.1787 | 0.1380	0.3863 | 0.3300	0.0421 | -0.1559	-0.3246 | -0.3684

Table 6: Dynamic parameters of the Concurrent Design (C.D.) and the Traditional Design (T.D.).

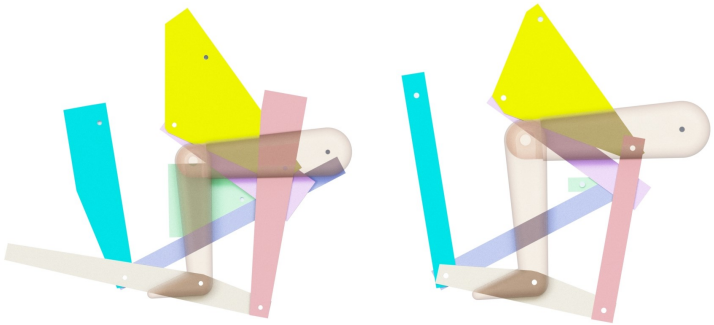

(a) Concurrent design. (b) Traditional design.

Figure 10: Obtained mechanism design by using both approaches.

In Table 7, the comparative results of the performance functions in the precision points for both designs are displayed. It is clear that both design approaches provide the same precision point tracking error $\bar{J}_1$. Nevertheless, the concurrent design decreases the total applied torque $\bar{J}_2$ with respect to the traditional design.

The last experiment includes the use of a Proportional-Integral (PI) controller to regulate the crank velocity to $\omega_2 = 2\pi\ rad/s$ with an applied force of $\vec{F}_{K_8} = [0, -133.41]^T N$ in the (x_E, y_E) coordinate of the mechanism. The same controller gains are considered in both designs for the numerical simulation with an integration time of $1ms$ and a final time of $3s$. The corresponding crank velocities, the applied torques, and the magnitudes of the total mass center in both designs are shown in Fig. 11. The velocity deviation in the steady-state in the C.D. is in the interval $[6.2458, 6.3504]$, while in the T.D. is in $[6.1849, 6.3605]$. A reduction of 40.43% is presented in the C.D.. The total mass centers of the mechanisms present fewer variations in the C.D. than the T.D.. This implies a reduction of the potential energy of the mechanism designed by the C.D., which results in a more efficient static balance. The energy consumption is also numerically provided in the last column of Table 7. It is important to note that the total power in the C.D. decreases 52.13% with respect to the T.D. in spite of having a larger total mass.

Hence, the simultaneous consideration of the kinematic synthesis and the dynamics into the design of the eight-bar mechanism results in a rehabilitation machine that consumes less energy, this can also reduce the control effort in the system in such a way that it decreases the error velocity. Also, the integration of the shape design in the proposed

J	$\bar{J}_1$ $[m^2]$	$\bar{J}_2$ $[N^2m^2]$	Energy [W]
C.D. | T.D.	C.D. | T.D.	C.D. | T.D.	C.D. | T.D.
1.9585×10^{-5} | 3.8159×10^{-5}	1.5399×10^{-5} | 1.5399×10^{-5}	4.1857 | 22.76	14.2018 | 29.6728

Table 7: Performance function and the energy consumption of the obtained rehabilitation mechanism with the Concurrent Design (C.D.) and the Traditional Design (T.D.).

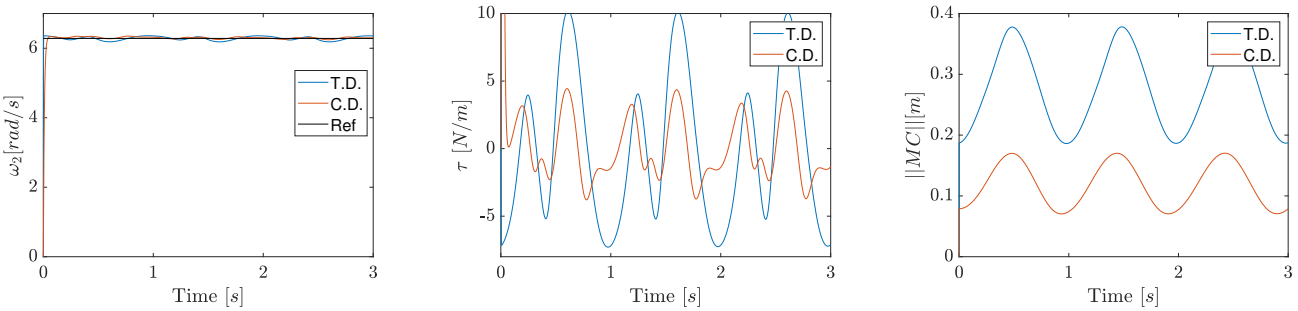

(a) Velocity behavior (b) Torque behavior. (c) Total mass center magnitude

Figure 11: Velocity behavior w_2, torque behavior τ and magnitude of total mass center $\|MC\|$ of the eight-bar mechanism with a PI velocity controller.

concurrent design approach can obtain real design solutions, i.e., it provides link shapes that can be manufactured. Suppose that only the mass, the inertia, and the mass center parameters (dynamic parameters) of the links are obtained as design solutions as in the case of [5]. Then, another optimization process is required to fit those solutions to specific link shapes, and it may produce unreal links or with significant differences in their dynamic parameters.

6. Conclusions

A methodology that integrates kinematic synthesis, structure shape design, and dynamic performance for rehabilitation machines is proposed and applied to a particular study case related to the eight-bar lower limb rehabilitation mechanism. Such design interactions in the concurrent design are stated as a nonlinear constrained dynamic optimization problem and solved via different DE variants to obtain the most suitable design solution. Considering that the mechanical structure is a load to be drive by the controller, the main characteristic of the proposed concurrent design is that it is designed so that the dynamic behavior presents less load, which results in less control effort, and so, the controller complexity may be reduced. It also gives the link shapes without requiring additional shape procedures.

The comparative analysis of the result provided by the proposed concurrent design with a traditional design approach shows that the integration of kinematic synthesis, structure shape design, and dynamic performance can notably influence the total power reduction at 52.13%, the velocity deviation in the steady-state at 40.43%, and in the implementation time. The latter because it provides real link shapes, i.e., it does not require time-consuming in another optimization process to fit the obtained inertial properties to specific link shapes. Therefore, the proposed concurrent design approach can generate an improved rehabilitation mechanism.

On the other hand, one important factor to be considered in this kind of design methodology is the use of efficient optimization algorithms such that they can also promote the synergy among design criteria. For the particular case,

among DE variants, the DER1B can efficiently explore and exploit the design space such that better reconfigurability in the rehabilitation mechanism design is achieved.

Acknowledgments

The authors acknowledge support from the Secretaría de Investigación y Posgrado del Instituto Politécnico Nacional (SIP-IPN) under project numbers $SIP-20180196$ and $SIP-20200150$ and $SIP-20200528$. The first author acknowledges support from the Mexican Consejo Nacional de Ciencia y Tecnología (CONACyT) through a scholarship to pursue graduate studies at CIDETEC-IPN.

Conflict of interest

The authors declare that there is no conflict of interest regarding the publication of this article.

CrediT authorship contribution statement

José Saúl Muñoz-Reina: Conceptualization, Methodology, Software, Validation, Formal analysis, Investigation, Roles/Writing - Original Draft, Writing - Review & Editing, Visualization. **Miguel G. Villarreal-Cervantes:** Conceptualization, Methodology, Validation, Investigation, Roles/Writing - Original Draft, Writing - Review & Editing, Supervision, Project administration, Funding acquisition, Visualization. **Leonel Corona-Ramírez:** Funding acquisition, Resources.

References

[1] M. Iosa, G. Morone, A. Fusco, M. Bragoni, P. Coiro, M. Multari, V. Venturiero, D. De Angelis, L. Pratesi, S. Paolucci, Seven capital devices for the future of stroke rehabilitation, Stroke research and treatment 2012 (2012).

[2] M. G. Villarreal-Cervantes, Approximate and widespread pareto solutions in the structure-control design of mechatronic systems, Journal of Optimization Theory and Applications 173 (2) (2017) 628–657.

[3] A. Rodríguez-Molina, M. G. Villarreal-Cervantes, M. Aldape-Pérez, An adaptive control study for the dc motor using meta-heuristic algorithms, Soft Computing 23 (3) (2019) 889–906.

[4] H. M. J. Van Brussel, Mechatronics-a powerful concurrent engineering framework, IEEE/ASME Transactions on Mechatronics 1 (2) (1996) 127–136.

[5] Q. Li, W. Zhang, L. Chen, Design for control-a concurrent engineering approach for mechatronic systems design, IEEE/ASME transactions on mechatronics 6 (2) (2001) 161–169.

[6] A. Mohebbi, S. Achiche, L. Baron, Integrated and concurrent detailed design of a mechatronic quadrotor system using a fuzzy-based particle swarm optimization, Engineering Applications of Artificial Intelligence 82 (2019) 192–206.

[7] M. Haemers, S. Derammelaere, A. Rosich, C. M. Ionescu, K. Stockman, Towards a generic optimal co-design of hardware architecture and control configuration for interacting subsystems, Mechatronics 63 (2019) 102275.

[8] M. G. Villarreal-Cervantes, C. A. Cruz-Villar, J. Alvarez-Gallegos, Synergetic structure–control design via a hybrid gradient-evolutionary algorithm, Optimization and Engineering 16 (3) (2015) 511–539.

[9] H.-S. Yan, G.-J. Yan, Integrated control and mechanism design for the variable input-speed servo four-bar linkages, Mechatronics 19 (2) (2009) 274 – 285.

[10] Z. Affi, B. EL-Kribi, L. Romdhane, Advanced mechatronic design using a multi-objective genetic algorithm optimization of a motor-driven four-bar system, Mechatronics 17 (9) (2007) 489 – 500.

[11] K. Seo, Z. Fan, J. Hu, E. D. Goodman, R. C. Rosenberg, Toward a unified and automated design methodology for multi-domain dynamic systems using bond graphs and genetic programming, Mechatronics 13 (8) (2003) 851 – 885.
[12] B. Feng, N. Morita, T. Torii, A new optimization method for dynamic design of planar linkage with clearances at joints—optimizing the mass distribution of links to reduce the change of joint forces, J. Mech. Des. 124 (1) (2002) 68–73.
[13] H. Azegami, L. Zhou, K. Umemura, N. Kondo, Shape optimization for a link mechanism, Structural and Multidisciplinary Optimization 48 (1) (2013) 115–125.
[14] D. Xu, G. Ananthasuresh, Freeform skeletal shape optimization of compliant mechanisms, J. Mech. Des. 125 (2) (2003) 253–261.
[15] L. K. Osterkamp, Current perspective on assessment of human body proportions of relevance to amputees, Journal of the American Dietetic Association 95 (2) (1995) 215–218.
[16] J. Pantoja-García, M. Villarreal-Cervantes, J. González-Robles, G. S. Cervantes, Síntesis óptima de un mecanismo para la marcha bípeda utilizando evolución diferencial, Revista Internacional de Métodos Numéricos para Cálculo y Diseño en Ingeniería 33 (1-2) (2017) 138–153.
[17] J. Pérez Orive, A. E. Pichardo, D. D. Chávez, Desarrollo de un estándar de marcha normal en hombres adultos, propuesta de estándar para normatividad en estudios de marcha de población mexicana, Rev. mex. ortop. traumatol 12 (5) (1998) 380–5.
[18] R. Storn, K. Price, Differential evolution–a simple and efficient heuristic for global optimization over continuous spaces, Journal of global optimization 11 (4) (1997) 341–359.
[19] M. B. Calva-Yáñez, P. A. Niño-Suarez, E. A. Portilla-Flores, J. A. Aponte-Rodríguez, E. Santiago-Valentn, Reconfigurable mechanical system design for tracking an ankle trajectory using an evolutionary optimization algorithm, IEEE Access 5 (2017) 5480–5493.
[20] J. S. Pantoja-García, M. G. Villarreal-Cervantes, C. V. García-Mendoza, V. M. Silva-García, Synergistic design of the bipedal lower-limb through multiobjective differential evolution algorithm, Mathematical Problems in Engineering 2019 (2019).
[21] S. Acharyya, M. Mandal, Performance of eas for four-bar linkage synthesis, Mechanism and Machine Theory 44 (9) (2009) 1784–1794.
[22] D. H. Wolpert, W. G. Macready, No free lunch theorems for optimization, IEEE Transactions on Evolutionary Computation 1 (1) (1997) 67–82.
[23] K. Deb, An efficient constraint handling method for genetic algorithms, Computer methods in applied mechanics and engineering 186 (2-4) (2000) 311–338.
[24] R. Drillis, R.J. Y Contini, Body segment parameters, Tech. rep., 1166.03, School of Engineering and Science, New York University. (1966).
[25] N. Palastanga, R. Soames, Anatomy and human movement: Structure and function, Elsevier, 2011.

José S. Muñoz-Reina received the B.S. degree in bionic engineering from the UPIITA-Instituto Politécnico Nacional (IPN) in 2015 at Mexico City and the M.Sc. in computer technology from CIDETEC-IPN in 2018 at Mexico City. He is currently a Ph.D. candidate in Robotic and Mechatronic System Engineering at CIDETEC-IPN. His research interest includes the optimal design of mechatronic systems.

Miguel G. Villarreal-Cervantes received the B.S. degree in electronics engineering, the M.Sc. and Ph.D. degrees in electrical engineering from the Center for Research and Advanced Studies (CINVESTAV), Mexico. He is a full-time professor at the IPN in Mexico since February 2010. His current research interests include mechatronic design based on bio-inspired optimization, optimal tuning with metaheuristic algorithms, and robotics.

Leonel G. Corona-Ramírez has a Mechanical Engineering Ph.D. in the Higher School of Engineering and Mechanics of the Instituto Politécnico Nacional (IPN-Mexico). Currently working as a research professor in the department of advanced technologies in the Interdisciplinary Professional Unit in Engineering and Advanced Technologies of the IPN. Among his contributions its remarkable authorships within the area of robotics and mechatronics.

Supplementary material

"Integrated design of a lower limb rehabilitation mechanism using differential evolution"

José Saúl Muñoz-Reina, M. G. Villarreal-Cervantes, Leonel Germán Corona Ramírez

Nomenclature

The paper adopts the following nomenclatures:

Parameter	Definition	Parameter	Definition
$\vec{l}_{\hat{s}}$ and $\vec{l}'_{\bar{s}}$	The $\hat{s}$-th and $\bar{s}$-th position vector	$l_{\hat{s}}$ and $l'_{\bar{s}}$	The $\hat{s}$-th and $\bar{s}$-th magnitude of position vector
$\theta_{\hat{s}}$ and $\theta'_{\bar{s}}$	The $\hat{s}$-sth and $\bar{s}$-sth direction of position vector	s	Link number
θ_2	Crank position	M_1 and M_2	Four-bar mechanism representation
M_3	Five-bar mechanism representation	$\hat{\theta}_s$	Offset angle
ω_s	The s-th angular velocity	j	Imaginary number
α_s	The s-th angular acceleration	x_s-y_s	Inertial coordinate
$\vec{lc}_s$	The s-th center of mass vector	δ_s	The s-th offset angle of the center of mass vector
lc_s	The s-th magnitude of the center of mass vector	$\vec{a}_{G_s}$	The s-th acceleration vector of the center of mass
$a_{G_{s_x}}$	The x component of the s-th $\vec{a}_{G_s}$ vector	$a_{G_{s_y}}$	The y component of the s-th $\vec{a}_{G_s}$ vector
x_{g_s}-y_{g_s}	The s-th coordinate axis in the center of mass	$\hat{k}$	Link node
$\vec{R}_{\hat{k}_s}$	The $\hat{k}$-th position vector in the s-th link	$R_{\hat{k}_{s_x}}$	The x component of the $\hat{k}$-th $\vec{R}_{\hat{k}_s}$ vector in the s-th link
$R_{\hat{k}_{s_y}}$	The y component of the $\hat{k}$-th $\vec{R}_{\hat{k}_s}$ vector in the s-th link	$\vec{F}_{\hat{k}_s}$	The $\hat{k}$-th force vector in the s-th link
$F_{\hat{k}_{s_x}}$	The x component of the $\hat{k}$-th $\vec{F}_{\hat{k}_s}$ vector in the s-th link	$F_{\hat{k}_{s_y}}$	The y component of the $\hat{k}$-th $\vec{F}_{\hat{k}_s}$ vector in the s-th link
m_s	The s-th link mass	g	Gravitational acceleration
I_{s_G}	The s-th moment of inertia	τ	Torque
$\check{X}$	Forces and torque vector	$\check{A}$	Matrix into the dynamics
$\check{B}$	Vector into the dynamics	$b_s, c_s, ..., ks$	Link edge length
ϕ_s	The s-th hole diameter	k	Simple geometry
m_{k_s}	The k-th mass in the s-th link	ρ_s	Material density
I_{k_s}	The k-th moment of inertia in the s-th link	$\bar{J}_1$ y $\bar{J}_2$	Terms of the objective function representing design objectives
J	Objective function	p	Design parameters vector
κ_1 y κ_2	Weights of the design objectives in the weighted sum	$[x_T, y_T]$	Desired precision points
$g_1, g_2, ..., g_{12}$	Inequality constraints	h_1, h_2	Equality constraints
$[x_{ini}, y_{ini}]$	Initial coordinate of the path	t	Time
$[\bar{x}_E, \bar{y}_E]$	Desired path points	$[x_E, y_E]$	Mechanism effector path
t_f	Final time	$\tilde{N}$	Number of precision points
$z_1, z_2, ..., z_8$	Collinear line with the link edge	σ_{vM}	Von Mises stress
$\bar{A}$, $\bar{B}$ y $\bar{C}$	Coefficients of the line equation	$\bar{D}$	Distance from a line to a point
$[x_{\hat{k}_s}, y_{\hat{k}_s}]$	Hole center coordinate	ζ_s	Distance between the hole and the link edges
σ_{k_s}	Stress in the hole	a_s	Contact area
Fc_{min}	Minimum security factor	σ_{adm}	Permissible stress
ψ_s	Minimum distance between holes	G	Generation
G_{max}	Max number of generations	x_i	Population
NP	Number of individuals	H	Height of a person
u_i	Child vector	D	Length of the design vector
cr	Crossover factor	F y K	Scale factors
L_l	Leg length	L_t	Thigh length
ξ	Coxofemoral joint angle	φ	Knee joint angle
$\tilde{p}_{ki}$	Kinematic parameters	$\tilde{p}_{sh}$	Shape parameters

Unknowns of the angular position analysis

The position vector loop unknowns θ_5, θ_6', θ_3, θ_4, θ_7 and θ_8 from equations (1)-(3) can be obtained applying the Euler's formula. Then, these are grouped to form Freudenstein's equations. The solution of Freudenstein's equations can be obtained as quadratic ones, therefore the unknowns are defined as follows:

$$\theta_5 = 2atan2\left(\frac{-\hat{B}_2 \pm \sqrt{\hat{B}_2^2 + \hat{A}_2^2 - \hat{C}_2^2}}{\hat{C}_2 - \hat{A}_2}\right) \tag{S1}$$

$$\theta_6' = 2atan2\left(\frac{-\hat{B}_1 \pm \sqrt{\hat{B}_1^2 + \hat{A}_1^2 - \hat{C}_1^2}}{\hat{C}_1 - \hat{A}_1}\right) \tag{S2}$$

$$\theta_3 = 2atan2\left(\frac{-\hat{B}_4 \pm \sqrt{\hat{B}_4^2 + \hat{A}_4^2 - \hat{C}_4^2}}{\hat{C}_4 - \hat{A}_4}\right) \tag{S3}$$

$$\theta_4 = 2atan2\left(\frac{-\hat{B}_3 \pm \sqrt{\hat{B}_3^2 + \hat{A}_3^2 - \hat{C}_3^2}}{\hat{C}_3 - \hat{A}_3}\right) \tag{S4}$$

$$\theta_7 = 2atan2\left(\frac{-\hat{B}_6 \pm \sqrt{\hat{B}_6^2 + \hat{A}_6^2 - \hat{C}_6^2}}{\hat{C}_6 - \hat{A}_6}\right) \tag{S5}$$

$$\theta_8 = 2atan2\left(\frac{-\hat{B}_5 \pm \sqrt{\hat{B}_5^2 + \hat{A}_5^2 - \hat{C}_5^2}}{\hat{C}_5 - \hat{A}_5}\right) \tag{S6}$$

where:

$$\hat{A}_1 = 2l_9 l_6' cos\theta_9 - 2l_2 l_6' cos\theta_2 \tag{S7}$$

$$l_{12} = \sqrt{l_1^2 + l_9^2 - 2l_1 l_9 cos(\theta_1 - \theta_9)} \tag{S8}$$

$$\hat{B}_1 = 2l_9 l_6' sin\theta_9 - 2l_2 l_6' sin\theta_2 \tag{S9}$$

$$\theta_{12} = atan2\left(\frac{l_1 cos\theta_1 - l_9 cos\theta_9}{l_1 sin\theta_1 - l_9 sin\theta_9}\right) \tag{S10}$$

$$\hat{C}_1 = l_9^2 + l_2^2 - l_5^2 + l_6'^2 - 2l_9 l_2 cos(\theta_9 - \theta_2) \tag{S11}$$

$$\theta_6' = \theta_6 + \hat{\theta}_6 \tag{S12}$$

$$\hat{A}_2 = -2l_9 l_5 cos\theta_9 + 2l_2 l_5 cos\theta_2 \tag{S13}$$

$$\hat{A}_5 = 2l_8 l_{12} cos\theta_{12} - 2l_6 l_8 cos\theta_6 + 2l_4 l_8 cos\theta_4 \tag{S14}$$

$$\hat{B}_2 = -2l_9 l_5 sen\theta_9 + 2l_2 l_5 sen\theta_2 \tag{S15}$$

$$\hat{B}_5 = 2l_8 l_{12} sin\theta_{12} - 2l_6 l_8 sen\theta_6 + 2l_4 l_8 sen\theta_4 \tag{S16}$$

$$\hat{C}_2 = l_9^2 + l_2^2 + l_5^2 - l_6'^2 - 2l_9 l_2 cos(\theta_9 - \theta_2) \tag{S17}$$

$$\tag{S18}$$

$$\hat{C}_5 = l_4^2 + l_6^2 + l_8^2 + l_{12}^2 - l_7^2 + 2l_4 l_{12} cos(\theta_4 - \theta_{12}) \tag{S19}$$

$$\hat{A}_3 = 2l_1 l_4 cos\theta_1 - 2l_2 l_4 cos\theta_2 - 2l_4 l_6 cos(\theta_4 - \theta_6) - 2l_6 l_{12} cos(\theta_6 - \theta_{12}) \tag{S20}$$

$$\hat{B}_3 = 2l_1 l_4 sen\theta_1 - 2l_2 l_4 sen\theta_2 \tag{S21}$$

$$\hat{A}_6 = -2l_4 l_7 cos\theta_4 + 2l_6 l_7 cos\theta_6 - 2l_7 l_{12} cos\theta_{12} \tag{S22}$$

$$\hat{C}_3 = l_1^2 + l_2^2 - l_3^2 + l_4^2 - 2l_1 l_2 cos(\theta_1 - \theta_2) \tag{S23}$$

$$\hat{B}_6 = -2l_4 l_7 sen\theta_4 + 2l_6 l_7 sen\theta_6 - 2l_7 l_{12} sin\theta_{12} \tag{S24}$$

$$\hat{A}_4 = -2l_1 l_3 cos\theta_1 + 2l_2 l_3 cos\theta_2 \tag{S25}$$

$$\hat{C}_6 = l_4^2 + l_6^2 + l_7^2 + l_{12}^2 - l_8^2 - 2l_4 l_6 cos(\theta_4 - \theta_6) \tag{S26}$$

$$\hat{B}_4 = -2l_1 l_3 sen\theta_1 + 2l_2 l_3 sen\theta_2 + 2l_4 l_{12} cos(\theta_4 - \theta_{12}) - 2l_6 l_{12} cos(\theta_6 - \theta_{12}) \tag{S27}$$

$$\hat{C}_4 = l_1^2 + l_2^2 + l_3^2 - l_4^2 - 2l_1 l_2 cos(\theta_1 - \theta_2) \tag{S28}$$

Unknowns of the angular velocity analysis

The velocity vector loop unknowns ω_2 - ω_8 from (4)-(6) can be obtained applying the Euler's formula. Separating the real and imaginary terms, these form a linear equation system. Solving the systems equations, the unknowns are defined as follows:

$$\omega_3 = -\frac{l_2 sin(\theta_2 - \theta_4)}{l_3 sin(\theta_3 - \theta_4)}\omega_2 \tag{S29}$$

$$\omega_4 = -\frac{l_2 sin(\theta_2 - \theta_3)}{l_2 sin(\theta_3 - \theta_4)}\omega_2 \tag{S30}$$

$$\omega_5 = -\frac{l_2 sin(\theta_2 - \theta'_6)}{l_5 sin(\theta_5 - \theta'_6)}\omega_2 \tag{S31}$$

$$\omega_6 = -\frac{l_2 sin(\theta_2 - \theta_5)}{l'_6 sin(\theta_5 - \theta'_6)}\omega_2 \tag{S32}$$

$$\omega_7 = -\frac{l_6 sin(\theta_6 - \theta_8)}{l_7 sin(\theta_7 - \theta_8)}\omega_6 + \frac{l_4 sin(\theta_4 - \theta_8)}{l_7 sin(\theta_7 - \theta_8)}\omega_4 \tag{S33}$$

$$\omega_8 = -\frac{l_6 sin(\theta_6 - \theta_7)}{l_8 sin(\theta_7 - \theta_8)}\omega_6 + \frac{l_4 sin(\theta_4 - \theta_7)}{l_8 sin(\theta_7 - \theta_8)}\omega_4 \tag{S34}$$

Unknowns of the angular acceleration analysis

The acceleration vector loop unknowns α_2 - α_8 from (7)-(9), can be obtained applying the Euler's formula. Separating the real and imaginary terms, the linear equation system is obtained. Solving the systems equations, the unknowns are defined as follows:

$$\alpha_3 = -\frac{l_2 cos(\theta_2 - \theta_4)\omega_2^2 + l_3 cos(\theta_3 - \theta_4)\omega_3^2 - l_4\omega_4^2}{l_3 sin(\theta_3 - \theta_4)} - \frac{l_2 sin(\theta_2 - \theta_4)}{l_3 sin(\theta_3 - \theta_4)}\alpha_2 \tag{S35}$$

$$\alpha_4 = -\frac{l_2 cos(\theta_2 - \theta_3)\omega_2^2 - l_4 cos(\theta_3 - \theta_4)\omega_4^2 + l_3\omega_3^2}{l_4 sin(\theta_3 - \theta_4)} - \frac{l_2 sin(\theta_2 - \theta_3)}{l_4 sin(\theta_3 - \theta_4)}\alpha_2 \tag{S36}$$

$$\alpha_5 = -\frac{l_2 cos(\theta_2 - \theta'_6)\omega_2^2 + l_5 cos(\theta_5 - \theta'_6)\omega_5^2 - l'_6\omega_6^2}{l_5 sin(\theta_5 - \theta'_6)} - \frac{l_2 sin(\theta_2 - \theta'_6)}{l_5 sin(\theta_5 - \theta'_6)}\alpha_2 \tag{S37}$$

$$\alpha_6 = -\frac{l_2 cos(\theta_2 - \theta_5)\omega_2^2 - l'_6 cos(\theta_5 - \theta'_6)\omega_6^2 + l_5\omega_5^2}{l'_6 sin(\theta_5 - \theta'_6)} - \frac{\alpha_2 l_2 sin(\theta_2 - \theta_5)}{l'_6 sin(\theta_5 - \theta'_6)} \tag{S38}$$

$$\begin{aligned}\alpha_7 =& \frac{l_4 cos(\theta_4 - \theta_8)\omega_4^2 - l_6 cos(\theta_6 - \theta_8)\omega_6^2 - l_7 cos(\theta_7 - \theta_8)\omega_7^2 + l_8\omega_8^2}{l_7 sin(\theta_7 - \theta_8)} \\ &+ \frac{l_4 sin(\theta_4 - \theta_8)}{l_7 sin(\theta_7 - \theta_8)}\alpha_4 - \frac{l_6 sin(\theta_6 - \theta_8)}{l_7 sin(\theta_7 - \theta_8)}\alpha_6\end{aligned} \tag{S39}$$

$$\begin{aligned}\alpha_8 =& \frac{l_4 cos(\theta_4 - \theta_7)\omega_4^2 - l_6 cos(\theta_6 - \theta_7)\omega_6^2 + l_8 cos(\theta_7 - \theta_8)\omega_8^2 - l_7\omega_7^2}{l_8 sin(\theta_7 - \theta_8)} \\ &+ \frac{l_4 sin(\theta_4 - \theta_7)}{l_8 sin(\theta_7 - \theta_8)}\alpha_4 - \frac{l_6 sin(\theta_6 - \theta_7)}{l_8 sin(\theta_7 - \theta_8)}\alpha_6\end{aligned} \tag{S40}$$

Position vectors $\vec{R}_{\hat{k}_s}$

The $\hat{k}-th$ position vectors $\vec{R}_{\hat{k}_s}$ in the $s-th$ link are described respect $s-th$ link mass center. According to the Free-body diagram in Fig.1(b), the polar representation are shown in (S41)-(S56).

$$\vec{R}_{C_2} = -lc_2 e^{j(\theta_2+\delta_2)} \tag{S41}$$

$$\vec{R}_{B_2} = l_2 e^{j\theta_2} + \vec{R}_{C_2} \tag{S42}$$

$$\vec{R}_{C_3} = -lc_3 e^{j(\theta_3+\delta_3)} \tag{S43}$$

$$\vec{R}_{B_3} = l_3 e^{j\theta_3} + \vec{R}_{C_3} \tag{S44}$$

$$\vec{R}_{C_4} = -lc_4 e^{j(\theta_4+\delta_4)} \tag{S45}$$

$$\vec{R}_{B_4} = l_4 e^{j\theta_4} + \vec{R}_{C_4} \tag{S46}$$

$$\vec{R}_{C_5} = -lc_5 e^{j(\theta_5+\delta_5)} \tag{S47}$$

$$\vec{R}_{B_5} = l_5 e^{j\theta_5} + \vec{R}_{C_5} \tag{S48}$$

$$\vec{R}_{C_6} = -lc_6 e^{j(\theta_6+\delta_6)} \tag{S49}$$

$$\vec{R}_{K_6} = l'_6 e^{j\theta'_6} + \vec{R}_{C_6} \tag{S50}$$

$$\vec{R}_{B_6} = l_6 e^{j\theta_6} + \vec{R}_{C_6} \tag{S51}$$

$$\vec{R}_{C_7} = -lc_7 e^{j(\theta_7+\delta_7)} \tag{S52}$$

$$\vec{R}_{B_7} = l_7 e^{j\theta_7} + \vec{R}_{C_7} \tag{S53}$$

$$\vec{R}_{C_8} = -lc_8 e^{j(\theta_8+\delta_8)} \tag{S54}$$

$$\vec{R}_{B_8} = l_8 e^{j\theta_8} + \vec{R}_{C_8} \tag{S55}$$

$$\vec{R}_{K_8} = l'_8 e^{j\theta_{11}} + \vec{R}_{C_8} \tag{S56}$$

The Cartesian form of position vectors (S41)-(S56) is obtained by applying the Euler's formula. With this representation is possible to use them directly in the dynamics equations (17)-(37)

Equations of inverse dynamic model

455 The dynamics equations (17)-(37) of the rehabilitation mechanism can be expressed as $\check{X} = \check{A}^{-1}\check{B}$ to form the inverse dynamic model. The matrix $\check{A} \in R^{21\times 21}$ can be expressed as shown in (S57), and the vector $\check{B} \in R^{21}$ is defined in (S58).

$$\check{A} = \begin{bmatrix}
1 & 0 & 1 & 0 & 0 & 0 & 0 & 0 & 0 & 0 & 0 & 0 & 0 & 0 & 0 & 0 & 0 & 0 & 0 & 0 & 0 \\
0 & 1 & 0 & 1 & 0 & 0 & 0 & 0 & 0 & 0 & 0 & 0 & 0 & 0 & 0 & 0 & 0 & 0 & 0 & 0 & 0 \\
-R_{C_{2_y}} & R_{C_{2_x}} & -R_{B_{2_y}} & R_{B_{2_x}} & 0 & 0 & 0 & 0 & 0 & 0 & 0 & 0 & 0 & 0 & 0 & 0 & 0 & 0 & 0 & 0 & 1 \\
0 & 0 & -1 & 0 & 0 & 0 & 1 & 0 & 0 & 0 & 0 & 0 & 0 & 0 & 0 & 0 & 0 & 0 & 0 & 0 & 0 \\
0 & 0 & 0 & -1 & 0 & 0 & 0 & 1 & 0 & 0 & 0 & 0 & 0 & 0 & 0 & 0 & 0 & 0 & 0 & 0 & 0 \\
0 & 0 & R_{C_{3_y}} & -R_{C_{3_x}} & 0 & 0 & -R_{B_{3_y}} & R_{B_{3_x}} & 0 & 0 & 0 & 0 & 0 & 0 & 0 & 0 & 0 & 0 & 0 & 0 & 0 \\
0 & 0 & 0 & 0 & 0 & 0 & -1 & 0 & 1 & 0 & 0 & 0 & 0 & 0 & 0 & 0 & 0 & 0 & -1 & 0 & 0 \\
0 & 0 & 0 & 0 & 0 & 0 & 0 & -1 & 0 & 1 & 0 & 0 & 0 & 0 & 0 & 0 & 0 & 0 & 0 & -1 & 0 \\
0 & 0 & 0 & 0 & 0 & 0 & R_{B_{4_y}} & -R_{B_{4_x}} & -R_{C_{4_y}} & R_{C_{4_x}} & 0 & 0 & 0 & 0 & 0 & 0 & 0 & 0 & R_{B_{4_y}} & -R_{B_{4_x}} & 0 \\
0 & 0 & -1 & 0 & -1 & 0 & 0 & 0 & 0 & 0 & 1 & 0 & 0 & 0 & 0 & 0 & 0 & 0 & 0 & 0 & 0 \\
0 & 0 & 0 & -1 & 0 & -1 & 0 & 0 & 0 & 0 & 0 & 1 & 0 & 0 & 0 & 0 & 0 & 0 & 0 & 0 & 0 \\
0 & 0 & R_{C_{5_y}} & -R_{C_{5_x}} & R_{C_{5_y}} & -R_{C_{5_x}} & 0 & 0 & 0 & 0 & -R_{B_{5_y}} & R_{B_{5_x}} & 0 & 0 & 0 & 0 & 0 & 0 & 0 & 0 & 0 \\
0 & 0 & 0 & 0 & 0 & 0 & 0 & 0 & 0 & 0 & -1 & 0 & 1 & 0 & 1 & 0 & 0 & 0 & 0 & 0 & 0 \\
0 & 0 & 0 & 0 & 0 & 0 & 0 & 0 & 0 & 0 & 0 & -1 & 0 & 1 & 0 & 1 & 0 & 0 & 0 & 0 & 0 \\
0 & 0 & 0 & 0 & 0 & 0 & 0 & 0 & 0 & 0 & R_{K_{6_y}} & -R_{K_{6_x}} & -R_{C_{6_y}} & R_{C_{6_x}} & -R_{B_{6_y}} & R_{B_{6_x}} & 0 & 0 & 0 & 0 & 0 \\
0 & 0 & 0 & 0 & 0 & 0 & 0 & 0 & 0 & 0 & 0 & 0 & 0 & 0 & -1 & 0 & 1 & 0 & 0 & 0 & 0 \\
0 & 0 & 0 & 0 & 0 & 0 & 0 & 0 & 0 & 0 & 0 & 0 & 0 & 0 & 0 & -1 & 0 & 1 & 0 & 0 & 0 \\
0 & 0 & 0 & 0 & 0 & 0 & 0 & 0 & 0 & 0 & 0 & 0 & 0 & 0 & R_{C_{7_y}} & -R_{C_{7_x}} & -R_{B_{7_y}} & R_{B_{7_x}} & 0 & 0 & 0 \\
0 & 0 & 0 & 0 & 0 & 0 & 0 & 0 & 0 & 0 & 0 & 0 & 0 & 0 & 0 & 0 & -1 & 0 & 1 & 0 & 0 \\
0 & 0 & 0 & 0 & 0 & 0 & 0 & 0 & 0 & 0 & 0 & 0 & 0 & 0 & 0 & 0 & 0 & -1 & 0 & 1 & 0 \\
0 & 0 & 0 & 0 & 0 & 0 & 0 & 0 & 0 & 0 & 0 & 0 & 0 & 0 & R_{B_{8_y}} & -R_{B_{8_x}} & -R_{C_{8_y}} & R_{C_{8_x}} & 0 & 0 & 0
\end{bmatrix} \tag{S57}$$

$$\check{B} = \begin{bmatrix}
m_2 a_{G_{2x}} \\
m_2 a_{G_{2y}} + m_2 g \\
I_{2_G}\alpha_2 \\
m_3 a_{G_{3x}} \\
m_3 a_{G_{3y}} + m_3 g \\
I_{3_G}\alpha_3 \\
m_4 a_{G_{4x}} \\
m_4 a_{G_{4x}} + m_4 g \\
I_{4_G}\alpha_4 \\
m_5 a_{G_{5x}} \\
m_5 a_{G_{5y}} + m_5 g \\
I_{5_G}\alpha_5 \\
m_6 a_{G_{6x}} \\
m_6 a_{G_{6y}} + m_6 g \\
I_{6_G}\alpha_6 \\
m_7 a_{G_{7x}} \\
m_7 a_{G_{7y}} + m_7 g \\
I_{7_G}\alpha_7 \\
m_8 a_{G_{8x}} - F_{K_{8_x}} \\
m_8 a_{G_{8x}} + m_8 g - F_{K_{8_y}} \\
I_{8_G}\alpha_8 - R_{K_{8_x}} F_{K_{8_y}} + R_{K_{8_y}} F_{K_{8_x}}
\end{bmatrix} \tag{S58}$$

Seat position

There are different ways to obtain the seat position, in this section, a method is presented based on the kinematics of lower limb. In (S59), the kinematic equations of the lower limb are expressed from $x_1 - y_1$ coordinate (see Fig. 8).

$$\begin{bmatrix} x_A + L_t cos(\theta_{L_t}) + L_l cos(\theta_{L_l}) - x_E \\ y_A + L_t sin(\theta_{L_t}) + L_l sin(\theta_{L_l}) - y_E \end{bmatrix} = \begin{bmatrix} 0 \\ 0 \end{bmatrix} \tag{S59}$$

where:

$$\begin{aligned} L_t &= 0.53H - 0.285H \\ L_l &= 0.285H - 0.039H \\ \theta_{L_t} &= -\Gamma - \xi \\ \theta_{L_l} &= -\varphi - \theta_{L_t} \end{aligned} \tag{S60}$$

First, the vertical displacement y_A of the seat position is obtained. This is considered fixed (with a constant value) and is obtained as follows:

1. Choose the average height of the Mexican population i.e $H = 1.7\ m$, and obtain the lower limb lengths L_t and L_l with (S60).
2. Find the minimum values of the x_E and y_E coordinates of the trajectory with respect to the $x_1 - y_1$ coordinate system. In the particular case such coordinates are $x_E = -0.4825$ and $y_E = -0.4182$.
3. Consider the lower limb is in the rest position (the thigh is collinear to the x_1 axis), i.e, the leg angle is $\varphi = -2\pi/9 rad$ (-40 degrees), the thigh angle is $\xi = 7\pi/18 rad$ (70 degrees) and the seat tilt is $\Gamma = 11\pi/18 rad$ (110 degrees); and compute the lower limb angles θ_{L_t} and θ_{L_l}.
4. Compute y_A using (S59). In this case $y_A = -0.1318\ m$.

Then, the x_A seat coordinate (horizontal displacement) is compute. This must be computed as a function of the human height H. Assuming the vertical displacement y_A is fixed, and using $sin(\theta_{L_l}) = \frac{-y_A + y_E}{L_l}$ obtained from the second equation of (S59) (considering the rest position in the lower limb), the x_A seat coordinate is given as,

$$x_A = -L_t cos(\theta_{L_t}) + L_l \sqrt{1 - \left(\frac{-y_A + y_E}{L_l} \right)^2} + x_E \tag{S61}$$

Considering the rest position in the lower limb (with the commented previous values in y_A, Γ, ξ φ, x_E and y_E), (S61) in terms of the human height H results,

$$x_A = 0.245H + 0.246H \sqrt{1 - \frac{1.194}{H^2}} - 0.4825 \tag{S62}$$

A linear equation which relates the human height H with the horizontal displacement of the seat x_A is presented in (S63). This is obtained by using a linear regression with the values presented with different heights H of the Mexican

population [S17] ($H \in [1.63\ m, 1.90\ m]$) in (S62).

$$x_A = 0.5589H - 0.6959 \tag{S63}$$

Note that the (x_A, y_A) coordinate represents the joint of the thigh. So, a small displacement in the negative direction of the vertical position is required to place the seat. In this work the displacement is set as $0.05\ m$ and it may be related to the half of the thigh clearance average (thigh thickness).